May 2017

An Elemental Highway: Investigation of a High Nickel Anomaly in Olivine from the Island of Niihau, Hawaii

Alexander James Valentine
University of Nevada, Las Vegas, alexjvalentine8@gmail.com

AN ELEMENTAL HIGHWAY: INVESTIGATION OF A HIGH NICKEL ANOMALY IN OLIVINE FROM THE ISLAND OF NIIHAU, HAWAII

By

Alexander J. Valentine

Bachelor of Science – Geology

University of California, Riverside

2015

A thesis submitted in partial fulfillment of the requirements for the

Master of Science – Geoscience

Department of Geoscience

College of Sciences

The Graduate College

University of Nevada, Las Vegas

May 2017

UNLV | GRADUATE COLLEGE

Thesis Approval

The Graduate College
The University of Nevada, Las Vegas

April 6, 2017

This thesis prepared by

Alexander J. Valentine

entitled

An Elemental Highway: Investigation of a High Nickel Anomaly in Olivine from the Island of Niihau, Hawaii

is approved in partial fulfillment of the requirements for the degree of

Master of Science – Geoscience
Department of Geoscience

Shichun Huang, Ph.D
Examination Committee Chair

Kathryn Hausbeck Korgan, Ph.D.
Graduate College Interim Dean

Arya Udry, Ph.D.
Examination Committee Member

Oliver Tschauner, Ph.D.
Examination Committee Member

Paul Forster, Ph.D.
Graduate College Faculty Representative

Abstract

The study of volcanic geochemistry is one of the main gateways for investigating the Earth's mantle. One important topic in the field is that of nickel (Ni) in the mineral olivine. While Ni is a compatible element in olivine, its high concentration at a given MgO content is not well understood. A variety of hypotheses have been proposed, including attributing presence of Ni to pyroxenite source melting, contribution from the core, or variation in peridotite source melting. In addition to the other hypotheses, chemical diffusion may also be a mechanism for enriching olivine Ni concentration. Magnesium-iron (Mg-Fe) isotopic measurements have been proposed as a test to see whether chemical diffusion occurs in olivine. Therefore, by taking Mg-Fe isotopic measurements of olivines, high Ni concentration in olivine can be attributed to either chemical diffusion or one of the other hypotheses.

To qualify which process led to Ni enrichment in olivine, this project analyzed olivines from basalt samples from the Hawaiian islands of Niihau, Kahoolawe, and Hawaii for major elemental and Mg-Fe isotopic content. Major elemental data have shown that Ni concentration at a given MgO content from olivines of the late-shield Paniau formation on Niihau is highest compared to global data. Mg-Fe isotopic data have shown that the olivines from Niihau follow diffusion models, indicating that chemical diffusion led to a high Ni concentration at a given MgO content. ~27 years of magmatic calibration at Niihau has been estimated by applying a diffusion model to in-situ data of an olivine phenocryst.

Acknowledgements

I thank my Advisor, Dr. Shichun Huang, for guiding me during my time at UNLV. Shichun provided me with not only incredible insight into the field of volcanic geochemistry, but engaged me into pursuing my goals in ways I have never thought of. Thanks to this, I was fortunate to have had an excellent experience in both my research and academic pursuits.

From UNLV, I thank Dr. Minghua Ren for use and assistance with the electron microprobe, Dr. Yuanxin Teng for assistance with bulk olivine collection, Dr. Arya Udry for assisting in sample imaging of the olivines, and Elise Nguyen for assistance in proofreading data. Their work truly helped me develop my project and allowed me to discover key details of my samples.

From USTC, I thank Dr. Fang Huang for hosting me during my visit. His equipment and advice regarding analysis of my samples were absolutely vital towards the success of my work. In addition, I thank all of his students for their incredible hospitality and assistance with my project. It strikes me as to how kind and helpful they had been to a new foreigner. I would also like to thank the National Science Foundation for funding my trip to China as part of the East Asia Pacific Summer Institute. This program is an absolute blessing to US graduate students working overseas and I am proud to have gone through the experience.

I thank my parents for allowing me to be where I am today. While I no longer have the opportunity to be with them through my current successes, I know that they would have been proud of what I have accomplished. Finally, I would like to thank my girlfriend, Erin Abendroth. She has assisted and encouraged me to succeed through both thick and thin, I am lucky to have had her by my side.

To my mother, Vivian (1954-2016), whose compassion, humor, and perseverance guided me through the difficulties and joys of life.

Table of Contents

List of Tables

List of Figures

Chapter 1: Introduction

Olivine [$(Mg,Fe)_2SiO_4$] is one of the most common phenocrysts in basalt; its study may help reveal clues relating to the dynamics of the Earth's mantle (Sobolev et al., 2005; Putirka et al., 2011; Teng et al., 2011; Herzberg et al., 2013). Ni is the most compatible element in olivine, with olivine having the largest Ni partition coefficient of any mantle silicate [~3.346; Beattie et al. (1991)]. Ni concentration in olivines derived from typical mantle peridotites is ~2000-3000 ppm (Herzberg et al., 2013). However, olivines in some basaltic lavas have been reported to have higher Ni concentrations at a given MgO content, some as high as ~4000-4750 ppm (Sobolev et al., 2005, 2007; Putirka et al., 2011). Typical mantle sources therefore do not explain the presence of such high Ni olivines; another source or process within the mantle is required to enrich Ni concentration at a given MgO content of olivine. Nonetheless, several hypotheses have been proposed.

It has been proposed that high Ni concentration at a given MgO content in olivine is the result of an olivine-free pyroxenite source (Sobolev et al. 2005; 2007). The formation of olivine-free pyroxenite originates from eclogite which has been formed by subducted crust within the mantle. Upon mantle convection, eclogite will come into contact with upwelling mantle peridotite as part of a mantle plume. Melting of this eclogite at shallow depths will produce high silica melts, which by reaction with olivines in the surrounding peridotite, will produce a secondary pyroxenite that is nearly devoid of olivine. While this secondary pyroxenite retains the Ni concentration of the peridotite parent, Ni will be less compatible with respect to peridotite. Consequentially, melts of this secondary pyroxenite will generate magmas that are highly enriched in Ni. Olivines crystallized from these magmas will therefore also become enriched in Ni, contrasting with olivines derived from typical mantle peridotites.

There are several other mantle sources which may produce high Ni concentration at a given MgO content in olivine. Ni enrichment in olivine can be attributed to a section (or sections) of the deep mantle that has interacted with the Earth's core (Herzberg et al, 2013). Consequentially, a mantle plume coming into contact with this source may accumulate a high Ni concentration. In addition, olivine Ni concentration may be enriched at given MgO content due to the presence of a large Ni variation in mantle peridotites (Putirka et al., 2011). A peridotite source that is high in Ni concentration, likely derived from deep melt extraction in the mantle or favorable temperature conditions promoting metasomatism, will therefore result in magmas crystallizing high Ni olivines at shallow depth.

Here, I propose another possible mechanism for generating high Ni concentration at a given MgO content in olivine. Chemical diffusion in olivine occurs when it is placed into a melt of differing MgO and FeO composition than that of its parental melt, thereby creating chemical zonation of MgO and FeO within olivine (Teng et al., 2011). If the new melt is of a lower MgO content, this will result in FeO enrichment and MgO depletion of the olivines (progressing from rim to core), leading to a net decrease in MgO content over time (**Figure 1C**). By comparison, NiO will diffuse at a similar rate alongside MgO, resulting in little change in Ni/Mg over varying MgO content (Petry et al., 2004). Instead, during fractional crystallization, Ni/Mg would decrease sharply with decreasing MgO content due to the high compatibility of Ni in olivine relative to Mg (Beattie et al., 1991). Upon eruption from this new melt, the crystallized olivines that have undergone chemical diffusion will retain a significantly higher Ni concentration at a given MgO content relative to typical mantle olivines.

I have tested each of these hypotheses using geochemical data of olivine grains from three locales around Hawaii: Niihau, Mauna Kea, and Kahoolawe (**Figure 2**). Three late-shield

lavas from the Ka’eo ridge intrusion at Niihau have high Ni concentrations, up to 1400 ppm at 12.5 wt % MgO (Cousens and Clague, 2015). Therefore, by analysis of Niihau olivines, the source or mechanism contributing to high Ni concentration at a given MgO content in olivine can be well constrained. Olivines from Mauna Kea and Kahoolawe were analyzed for comparison.

Chapter 2: Samples

Olivines from each study location (Niihau, Mauna Kea, and Kahoolawe) were selected for bulk analysis, including Mg-Fe isotopic measurements and major elemental measurements (a detailed sample list with comments is in **Table A2-1** of **Appendix A2**). Additional olivines from Niihau were also selected for in-situ electron microprobe analysis.

Niihau:

- 11 olivine grains from a basalt whole-rock (75-Nii-4) of the late-shield stage Paniau formation (located on Ka'eo ridge) were selected for bulk analysis (**Figure 3A**).

- 13 olivine grains within two basalt whole-rocks (75-Nii-1 and 75-Nii-2) of the same formation were selected for electron microprobe analysis (**Figure 3B**).

Mauna Kea:

- 20 olivine grains from a basalt whole-rock (HSDP-2 Unit 284) recovered by the Hawaii Scientific Drilling Project 2 (HSDP-2) were selected for bulk analysis (**Figure 3C**).

Kahoolawe:

- 22 olivine grains from a basalt whole-rock (Kah-16) were selected for bulk analysis (**Figure 3D**).

Olivine grains used for bulk analysis were hand-picked from the crushed whole-rocks. The coarse grains were transferred into small cylindrical containers, which were placed under a petrographic microscope. Milli-Q (MQ) H_2O was added to the containers to clean out remaining whole-rock and strengthen grain luster during visual inspection. Olivines were picked with a

preference for grains containing a negligible amount of melt inclusions and alterations (i.e. <5% of the overall olivine volume). They were also inspected for size and weighed on a scale, with a preference for retaining olivines >0.5 mm in diameter and >0.5 mg in weight. Prior to analysis, the olivine grains were wrapped into pieces of parafilm and placed within capped microcentrifuge tubes.

Chapter 3: Analyses

3.1 - Summary

Analyses conducted included in-situ major elemental measurements using an electron microprobe, bulk-mineral major elemental measurements using an inductively-coupled plasma mass spectrometer (ICP-MS) by solution, and bulk-mineral Mg-Fe isotopic measurements using a multi-collector inductively-coupled plasma mass spectrometer (MC-ICP-MS) by solution. In-situ olivine measurements were conducted on olivine phenocrysts within polished whole-rock samples at the University of Nevada, Las Vegas (UNLV) Electron Microanalysis and Imaging Laboratory (EMiL). Bulk sample measurements were done at the Chinese Academy of Sciences (CAS) Key Laboratory of Crust-Mantle Materials and Environments at the University of Science and Technology of China (USTC).

3.2 - Electron microprobe major elemental analysis

In-situ major elemental analysis was conducted on a JEOL JXA-8900 Electron Probe Microanalyzer (EPMA) at UNLV for olivines in Niihau basalt whole-rock samples 75-Nii-1 and 75-Nii-2. Prior to analysis, the basalt samples were cut into rectangular prisms, polished, and carbon coated. After whole-section X-ray maps were collected, the basalts were inspected for ideally sized olivine phenocrysts and transverse lines were plotted alongside crystal diameter in order to adjust for possible chemical zonation. The 13 phenocrysts measured are on average 1 mm in diameter, with 30 μm diameter or 50 μm diameter spot analyses. The groundmass of sample 75-Nii-1 was also measured. Analysis was conducted at a 100 nA current and 15 kV accelerating voltage. Thallium acid phthalate (TAP) and lithium fluoride (LiF) crystals were

used in wavelength dispersive X-ray spectroscopy (WDS) for the analyzed elements (MgO, SiO_2, FeO, MnO, and NiO). Each element was calibrated relative to the following standards: Geller 3N Mg crystal for MgO, Geller 5N Si crystal for SiO_2, NMNH 96189 (illmenite) for FeO and MnO, and synthetic Ni-olivine for NiO. Long-term external precision was determined by repeated analyses of NMNH 111312-44 (San Carlos olivine) and USNM 2566 (Springwater olivine) standards. Standard information, precision, WDS crystal, and counting time for each element are summarized in **Table A1-1** of **Appendix A1**. Major elemental oxide values (in wt %) were calculated and corrected using the ZAF (i.e. atomic number, absorbance, and fluorescence) matrix correction method on the instrument's software.

3.3 - Bulk olivine analyses

3.3.1 - Olivine dissolution

Sample dissolution was conducted prior to analysis in a clean laboratory at USTC (dark blue boxes of **Figure 4**). The 53 olivine samples from basalt whole-rocks 75-Nii-4, HSDP-284, and Kah-16 were first transferred into pre-cleaned 7 mL Teflon beakers, where they were dissolved in a mixture of concentrated HNO_3 (0.5 mL for <5 mg samples and 1 mL for >5 mg samples) and HF (1.5 mL for <5 mg samples and 3 mL for >5 mg samples). To obtain a better dissolution, the capped beakers were placed into an ultrasonic bath for ~15 minutes. After the initial digestion and evaporation to dryness, the samples were treated with 2.4 mL aqua regia (1:3 molar HNO_3:HCl) and dried again. For each step, the capped beakers were heated at a temperature of ~140^{o}C on a hot plate for 1-2 days. Finally, ~0.07-0.6 mL 6N HCl was added to

each sample; depending on concentration, samples were grouped into 50 μg Fe, 20 μg Fe, or <20 μg Fe analysis stock solutions for the bulk sample measurements (orange boxes of **Figure 4**).

3.3.2 – Solution ICP-MS major elemental analysis

Major elemental analysis of the 53 olivine sample solutions was conducted on a PerkinElmer ELAN II ICP-MS at USTC. The stock solutions were first evaporated and 2 mL 1.2N HNO_3 was added to each sample (light blue boxes of **Figure 4**). 0.05 mL aliquots were then taken and diluted to 5 mL by addition of 4.95 mL MQ H_2O prior to analysis. The diluted sample solutions were introduced directly to the instrument through a Teflon sample inlet, with approximately 30 seconds allotted per sample run. Intermittent 2% HNO_3 rinse was conducted following each analysis to prevent sample cross-contamination. An instrumental blank, linearity standards (5, 10, 50, 100, 500, 1000, and 5000 ppb Mg and Fe), and 5 whole-rock standards (BHVO-2, DTS-2, PCC-1, BCR-2, and BIR-1) were run prior to unknown samples. Data output was in the form of six spreadsheets, consisting of Mg and Fe count intensity and time (in seconds) data. Count rate data were corrected for the instrumental blank and converted to absolute (ppb) concentration by correlation with the linearity standards. Forsterite content was calculated using Fo = molar Mg / (Fe + Mg) * 100.

3.3.3 - Purification of Fe for isotopic analysis

Fe was purified by ion-exchange chromatography in a clean laboratory at USTC (peach boxes of **Figure 4**). Columns were first loaded with 0.5 mL Bio-Rad AG 1-X8 anion exchange

resin, which was kept humid in MQ H_2O. The columns were cleaned with subsequent 1 mL rinses of 8N HNO_3, 1N HNO_3, 0.4N HCl, and 6N HCl, with a 2 mL MQ H_2O rinse prior to and between each acid rinse. Once the columns were drained, 0.2 mL of the 6N HCl 50 μg Fe and 20 μg Fe sample solutions (with 0.4 mL of solution introduced instead for samples <20 μg Fe) were loaded onto the columns. This was followed by elution of Fe with 4 mL 6N HCl, during which the samples matrices were removed. Purified Fe was then collected into pre-cleaned 7 mL Teflon beakers using 0.4N HCl (2 times with 0.5 mL and 3 times with 1 mL), 1 mL 8N HNO_3, and 0.5 mL MQ H_2O run through the columns. The purified Fe solutions were evaporated on a hotplate for isotopic analysis.

3.3.4 - Purification of Mg for isotopic analysis

Mg was purified by ion-exchange chromatography in a clean laboratory at USTC following the elution procedure of An et al. (2014) (green boxes of **Figure 4**). The remaining 1.95 mL sample stock solutions were weighed, transferred to 20 mL Teflon beakers, evaporated, and ~0.1-14 mL 1.2N HNO_3 was added to obtain >1.5 mg Mg or <1.5 mg Mg sample solutions for analysis. The columns were loaded with 2 mL Bio-Rad AG 50W-X12 cation exchange resin, kept humid in MQ H_2O, and cleaned three times with 4 mL 4N HNO_3 + 0.5N HF prior to purification. The columns were then conditioned using 6 mL 1.2N HNO_3 and 0.1 mL of the 1.2N HNO_3 sample solutions were loaded. Sample matrices were washed using 17 mL 1.2N HNO_3. Purified Mg was then collected into pre-cleaned 20 mL Teflon beakers using 18 mL 1.2N HNO_3 run through the columns. The Mg solutions were passed through the column twice. The purified Mg solutions were then evaporated for isotopic analysis.

3.3.5 - Solution MC-ICP-MS Fe isotopic analysis

Fe isotopic analysis was conducted on a Thermo Scientific Neptune Plus MC-ICP-MS at USTC using a quartz dual cyclonic spray chamber and PFA MicroFlow Teflon nebulizer following the procedure of Gong et al. (2016). 2 mL 2% HNO_3 was added to the dried purified Fe samples to obtain ~2 ppm Fe solutions for analysis. Fe isotopes were measured using the sample-standard bracketing method and each sample was analyzed three times. Elemental Fe standard IRMM-014 was used for each analysis. Between sample measurements, the sample inlet system was rinsed three times with 5% and 2% HNO_3 to ensure a negligible ^{54}Fe signal (i.e. <1 mV) prior to the next analysis. ^{54}Fe, ^{56}Fe, ^{57}Fe, and ^{58}Fe data were measured in static mode on L1, C, H1, and H2 Faraday cups, respectively. Contributions from isobaric interferences (i.e. $^{40}Ar^{14}N$ on ^{54}Fe and $^{40}Ar^{16}O$ on ^{56}Fe) were eliminated by measuring at high resolution mode with an M/ΔM of ~8900. $\delta^{56}Fe_{IRMM\text{-}014}$ values {defined as $\delta^{56}Fe_{IRMM\text{-}014}$ (‰) = $[(^{56}Fe/^{54}Fe)_{olivine} / (^{56}Fe/^{54}Fe)_{IRMM\text{-}014} - 1] * 1000$} were calculated after taking the average of the three duplicate analyses. The precision and accuracy of the Fe isotopic measurements were estimated by long-term measurement of 7 whole-rock USGS standards (RGM-2, GA, GS-N, AGV-2, BCR-2, DTS-1, and PCC-1) and 2 in-house Fe standards (UIFe and GSB-1). As seen in Table S1 of An et al. (2017), the data from the instrument show consistency with the literature Fe values.

3.3.6 - Solution MC-ICP-MS Mg isotopic analysis

Mg isotopic analysis was conducted on a Thermo Scientific Neptune Plus MC-ICP-MS at USTC using a quartz dual cyclonic spray chamber and PFA MicroFlow Teflon nebulizer following the procedure of An et al. (2014). 2 mL 2% HNO_3 was added to the dried purified Mg

samples to obtain ~2 ppm Mg solutions for analysis. Mg isotopes were measured using the sample-standard bracketing method and each sample was analyzed three times. Mg nitrate standard DSM-3 was used for each analysis. Between sample measurements, the sample inlet system was rinsed three times with 5% and 2% HNO_3 to ensure a negligible ^{24}Mg signal (i.e. <1 mV) prior to the next analysis. ^{24}Mg, ^{25}Mg, and ^{26}Mg data were measured in static mode on L3, C, and H3 faraday cups, respectively. Analysis was conducted on medium to high resolution mode with an M/ΔM of ~5000-8000. $\delta^{26}Mg_{DSM-3}$ values {defined as $\delta^{26}Mg_{DSM-3}$ (‰) = $[(^{26}Mg/^{24}Mg)_{olivine} / (^{26}Mg/^{24}Mg)_{DSM-3} -1] * 1000$} were calculated after taking the average of the three duplicate analyses. The precision and accuracy of the Mg isotopic measurements were estimated by long-term measurement of 7 whole-rock USGS standards (RGM-2, GA, GS-N, AGV-2, BCR-2, DTS-1, and PCC-1) and 3 in-house Mg standards (CAM-1, SRM980, and IGGMg1). As seen in Table S1 of An et al. (2017), the data from the instrument show consistency with the literature Mg values.

Chapter 4: Results

4.1: Electron microprobe data

In-situ major elemental data are compiled in **Tables A1-2** and **A1-3** of **Appendix A1**. The average SiO_2 (wt %), MgO (wt %), FeO (wt %), MnO (wt %), NiO (wt %), and Fo (#) compositions of the in-situ olivines are 39.61, 42.86, 17.58, 0.19, 0.38, and 81.30, respectively. The olivines have a large degree of elemental zoning, producing smooth curves with high MgO and NiO compositions at the cores and high FeO composition at the rims (**Figure 5**). Comparing to basalt whole-rock from Niihau and Kauai islands, the olivines measured have a considerably high variation in Ni concentration (~1750 to 4000 ppm) at a given MgO content (~35-45 wt %) (**Figure 6**). This is consistent with the findings of Cousens and Clague (2015), in which high Ni concentration at a given MgO content was reported in basalt whole-rocks at Niihau.

Figure 7 shows the trend of Fo content vs. NiO in an olivine phenocryst at Niihau (75-Nii-2-8) relative to the global trend of olivine compositions. Similar to **Figure 6**, NiO plots highest at a given Fo content for Niihau (NiO being ~0.25 to 0.5 wt %), with the range of Fo content covered for NiO at Niihau between 70 to 85 (global NiO composition is only equivalent at ~5 Fo # higher). One exception are the olivines from Norilsk, Siberia [from Sobolev et al. (2007); light blue boxes of **Figure 7**], which plot on a similar trend to those from Niihau.

4.2: Bulk olivine Mg-Fe isotopic and major elemental data

Bulk olivine major elemental (Fo content) and Mg-Fe isotopic data are compiled in **Table A2-2** of **Appendix A2**. For Niihau bulk olivines, the average $\delta^{56}Fe_{IRMM\text{-}014}$ (‰),

$\delta^{57}Fe_{IRMM-014}$ (‰), $\delta^{25}Mg_{DSM-3}$ (‰), $\delta^{26}Mg_{DSM-3}$ (‰), and Fo (#) compositions are -0.86, -1.29, 0.04, 0.08, and 79.82, respectively. Aligning with the standard data, the positive correlation of $\delta^{56}Fe_{IRMM-014}$ vs. $\delta^{57}Fe_{IRMM-014}$ (**Figure 8**) and $\delta^{25}Mg_{DSM-3}$ vs. $\delta^{26}Mg_{DSM-3}$ (**Figure 9**) in the olivine data ensures that the isotopic measurements are of good quality. In addition, there is consistency with the olivine values of Teng et al. (2011) and Sio et al. (2013), with the values measured here constrained within their variability. For the measured olivines, $\delta^{26}Mg_{DSM-3}$ values are negatively correlated with $\delta^{56}Fe_{IRMM-014}$ (**Figure 10**). This is especially inherent for the olivines from Niihau, where Fe is considerably lighter (i.e. negative $\delta^{56}Fe_{IRMM-014}$) and Mg is considerably heavier (i.e. positive $\delta^{26}Mg_{DSM-3}$). The Mg-Fe isotopic data are aligned consistently with the data of Teng et al. (2011) and Sio et al. (2013), having a similar negative correlation of olivine Fe and Mg isotopic compositions.

Chapter 5: Discussion

5.1 - Elemental zoning within olivine

5.1.1 - Formation of elemental zoning in olivine

The Niihau olivines are zoned in both MgO and FeO content, with progressively increasing MgO and decreasing FeO occurring towards the olivine cores (**Figure 5**). Elemental zoning within olivine has been attributed to fractional crystallization, a process in which olivine forming in a melt will effectively grow and equilibrate to the changing composition of the melt over time (i.e. Pearce, 1987; **Figure 1A**). It can also be produced by chemical diffusion, which involves movement of formed homogenous olivine into a melt of differing composition (**Figure 1C**). This results in re-equilibration of the olivine composition to the new melt and forms elemental zonation by inverse transfer of Mg and Fe (Dauphas et al., 2010). In addition, if olivine grows quickly enough, diffusion-limited crystal growth may also lead to elemental zoning (Welsch et al., 2014; Shea et al., 2015; **Figure 1B**). This is dependent on the high rate of chemical diffusion in a melt relative to a homogeneous olivine core, where a diffusive boundary layer will accommodate elements based on their magma diffusion rate (with Mg being incorporated faster than Fe into olivine) (Oeser et al., 2015).

Mg and Fe isotopic measurements have been recently proposed to test which of these processes forms elemental zoning in olivine (Dauphas et al., 2010; Teng et al., 2011). If the isotopes of these elements are fractionated within olivine, this would indicate that fractional crystallization is not the cause for elemental zoning, as there should be little to no magmatic isotopic fractionation. Teng et al. (2011) found coupled Mg and Fe isotopic fractionation present in some Hawaiian olivines. In addition to ruling out fractional crystallization due to the presence

of isotopic fractionation, this result was also inconsistent with rapid crystal growth due to the negatively correlated (rather than unidirectional) fractionation of Mg and Fe isotopes (**Figure 1B**). It was therefore proposed that chemical diffusion generated elemental zoning in the Hawaiian olivines.

As discussed in Chapter 1, Ni diffuses similarly in rate and direction to Mg in olivine, their diffusion coefficients D_{Ni} and D_{Mg} varying from ~1 x 10^{-15} to ~1 x 10^{-19} m^2/s (Chakraborty, 1997; Petry et al., 2004). Therefore, for olivines undergoing chemical diffusion, assuming that the olivine is of a higher original Fo content than that of the melt, Ni/Mg will have little variation with decreasing Fo. This results in these olivines having higher Ni concentrations at a given MgO content relative to olivines undergoing fractional crystallization, where Ni/Mg is expected to greatly decrease due to the higher compatibility of Ni in olivine relative to Mg.

5.1.2: Modeling olivine elemental zoning

Assuming that chemical diffusion resulted in the elemental zoning of the studied Niihau olivines, the timeline of diffusion for each mobile element in olivine (i.e. Mg, Fe, and Ni) can be established (Teng et al., 2011; Sio et al., 2013; Oeser et al., 2015; Hartley et al., 2016). **Figure 5** shows elemental profiles of Niihau olivine 75-Nii-2-8 plotted alongside chemical diffusion models of varying timescales. The chemical diffusion models are based off of a partial differential equation governing non-steady state spherical diffusion with a constant surface concentration (i.e. Eq. 6.18 of Crank, 1975 and Eq. 8.6.7 of Albaréde, 1996; see **Appendix C**). Given an initial olivine and melt composition estimated for olivine 75-Nii-2-8 (see **Table C3** of **Appendix C** for parameters), each element will equilibrate over time based off of an

experimentally defined diffusion coefficient (i.e. Chakraborty, 1997; Petry et al., 2004; Dohmen and Chakraborty, 2007). It is expected that the originally homogenous olivine will drop in MgO composition and increase in FeO composition at the rims (i.e. following the 1 month and 1 year diffusion models). Eventually, after 10000 days (~27 years), the profiles become rounded compared to the previous pseudo-rectangular shape and the elemental profiles seen in the olivine can be reproduced. Given more time, the core of the olivine would start changing composition (i.e. following the 50 year diffusion model). The bottom profile of **Figure 5** shows the corresponding Mg and Fe isotopic fractionation associated with each of these timescales. Assuming that this olivine was equilibrated following the expected timescale (10000 days or ~27 years), Mg and Fe isotopic fractionation should be relatively strong, following a twin-peak (for Mg) and twin-valley (for Fe) profile.

To determine whether chemical diffusion or fractional crystallization was present at Niihau, the olivine microprobe data was compared to models of both processes. **Figure 7** shows two fractional crystallization models and two diffusion models plotted alongside the data. The fractional crystallization models are adopted from that of Putirka et al. (2011) (see **Appendix B**), with one of the models adjusted to the Fo content of an olivine core composition at Niihau (olivine 75-Nii-2-8; dark red line of **Figure 7**) and the other adjusted to the global average (green line of **Figure 7**). As mentioned earlier, the chemical diffusion models are based on that of non-steady state spherical diffusion (i.e. Crank, 1975 and Albaréde, 1996; see **Table C3** of **Appendix C** for parameters). The chemical diffusion models are equilibrated to the high and low Fo compositions of Niihau (light red line of **Figure 7**) and Massif Central, France [pink line of **Figure 7**; from Oeser et al., (2015)] using the estimated in-situ timescale of olivine 75-Nii-2-8

(~27 years). Olivines from Massif Central have been shown to be controlled by chemical diffusion (Oeser et al., 2015).

In **Figure 7**, olivines from Niihau and Massif Central plot consistently with their diffusion-controlled Fo-NiO trends. Interpreted by Sobolev et al. (2007) to be derived from a nearly pure (~100%) pyroxenite source, the olivines from Norilsk plot at a similar slope to the Niihau diffusion model. Derived from thick continental WPM (within plate magmas), it is likely that the origin of high Ni concentration in olivines at Norilsk may have been attributed to a specific mantle source. Nevertheless, from its shallow Fo-NiO trend, its most recent event in magmatic equilibration was likely that of chemical diffusion. By comparison, the fractional crystallization model trends are considerably steeper. One issue with the diffusion model is that it does not explain the original source of high Ni concentration (i.e. NiO concentration towards the highest Fo olivines of each sample set within **Figure 7**). Rather, it indicates that the elemental zoning present within the modeled olivines must have been formed by chemical diffusion during their most recent magmatic event. More importantly, for the sample sets observed, it explains the presence of anomalously high Ni concentrations at given MgO content. While the models are well-fitted, presence of chemical diffusion as a primary process enriching Ni concentration at a given MgO content can only be confirmed through isotopic analysis of the olivines.

5.2 - Test of Ni enrichment hypotheses

5.2.1 - Expected isotopic observations

In order to qualify each of the hypotheses for olivine Ni enrichment, the olivine Mg-Fe isotopic data will be compared to their expected patterns of isotopic fractionation. The following observations are expected based on each hypothesis presented in Chapter 1 (an example of each trend is shown in **Figure 11**):

Secondary pyroxenite: If negative $\delta^{56}Fe$ isotopic values with little to no Mg fractionation are observed within the measured olivines, the presence of high Ni concentration at a given MgO content is the result of a secondary pyroxenite source. This would be consistent with what is seen on the nearby island of Koolau, where whole-rock samples with considerably low CaO content are likely derived from a pyroxenite source (Sobolev et al., 2005; Teng et al., 2013).

Variation of Ni in peridotite: If the measured Mg-Fe isotopic values for the olivines show a large degree of scatter or offset from typical mantle values, the presence of high Ni concentration at a given MgO content can be explained by a Ni-rich mantle peridotite source. This is consistent with a peridotite source which has undergone large changes in temperature and metasomatism relative to ambient mantle (Putirka et al., 2011). As $\delta^{56}Fe_{IRMM\text{-}014}$ vs. $\delta^{57}Fe_{IRMM\text{-}014}$ (**Figure 8**) and $\delta^{25}Mg_{DSM\text{-}3}$ vs. $\delta^{26}Mg_{DSM\text{-}3}$ (**Figure 9**) olivine data appear to be positively correlated, it is unlikely that this hypothesis may be supported here, as significant scatter or offset from typical mantle values for each isotope should be expected.

Out-core signature: If the olivines have little to no Mg-Fe isotopic fractionation, consistent with a typical mantle-like signature, the presence of high Ni concentration at a given

MgO content may reflect an out-core signature. This is explained by relatively low degrees of isotopic fractionation of these elements (i.e. average mantle $\delta^{56}Fe_{IRMM-014} = 0 \pm 0.1‰$ and average mantle $\delta^{26}Mg_{DSM-3} = -0.3 \pm 0.2‰$) during the formation of the core (Dauphas et al., 2009; 2010). $^{3}He/^{4}He$ measurements of the olivines would also need to be conducted to allow for further comparison with the model proposed by Herzberg et al. (2013). This is due to the fact that ^{3}He is a primordial isotope of He, with $^{3}He/^{4}He$ gradually decreasing through radioactive decay to ^{4}He (from α-decay) with time after the formation of the solar system. It is assumed that olivines high in $^{3}He/^{4}He$ are derived from a deep mantle source that has been incompletely degassed in ^{3}He. $^{186}Os/^{188}Os$ and $^{187}Os/^{188}Os$ olivine data would also provide a further constraint. Pt/Os and Re/Os are assumed to be enriched within the outer core, where ^{186}Os and ^{187}Os are derived from the radiogenic isotopes ^{190}Pt and ^{187}Re, respectively. Olivine samples displaying high $^{186}Os/^{188}Os$ and $^{187}Os/^{188}Os$ would therefore also indicate deep mantle derivation (Brandon et al., 2003).

Chemical diffusion: Previous research has shown that diffusion results in Mg-Fe isotopic zoning of olivines (Dauphas et al., 2010; Teng et al., 2011; Sio et al., 2013; Oeser et al., 2015). This process occurs when an olivine is transferred into a melt of lower MgO and higher FeO composition, creating a sharp compositional contrast between the olivine and melt (i.e. **Figure 1C**). Mg will diffuse into the melt from the olivine with Fe travelling conversely (with diffusion coefficient D_{Mg-Fe} varying from $\sim 1 \times 10^{-15}$ to $\sim 1 \times 10^{-19}$ m^2/s) until equilibrium is reached. Undergoing kinetic fractionation, ^{24}Mg will diffuse out of the olivine faster than ^{26}Mg and ^{54}Fe will diffuse into the olivine faster than ^{56}Fe, as lighter isotopes of these elements will travel faster. This results in relatively positive $\delta^{26}Mg$ and negative $\delta^{56}Fe$ signatures progressing

across crystal diameter. If this isotopic pattern is seen in the data, it is likely that the enrichment of Ni at a given MgO content occurred as a consequence of this process.

Based on these expected observations, the Mg-Fe isotopic data from this project will be compared in order to determine which hypothesis likely resulted in Ni enrichment of olivine at Niihau.

5.2.2 - Interpretation of Mg-Fe isotopic data

Niihau olivine Mg and Fe isotopic compositions are negatively correlated (**Figure 10**), which is consistent with chemical diffusion generating high Ni concentration at given MgO content in olivine. By comparison with the expected isotopic trend of chemical diffusion from **Figure 11**, the olivine data of **Figure 10** plot similarly. Comparing to radial and bulk diffusion models (see **Tables C3** and **C4** of **Appendix C**, respectively, for parameters), the olivine data also plot at a similar negative slope. Similar to radial diffusion, bulk diffusion determines the mean concentration of a given sphere rather than concentration across sphere radius [i.e. Eq. 8.6.7 of Albaréde (1996)]. From the bulk diffusion model, the olivines will undergo increasing fractionation upon placement into the new melt. They will then reverse fractionation trend at ~35 years and obtain less fractionated values as before until the olivines reach equilibrium with the melt. The data illustrates that chemical diffusion generated elemental zoning in the olivines and that Ni was enriched following this pattern. This is notable in that not only was Ni at Niihau enriched at a given MgO content by chemical diffusion, but that for each location studied, this set of isotopic data are consistent with the literature data confirming chemical diffusion in the formation of olivine (i.e. Teng et al., 2011; Sio et al., 2013; Oeser et al., 2015).

Chapter 6: Conclusions and implications

This study investigated the formation of high Ni concentration at a given MgO content in olivine at Niihau, Hawaii. Several hypotheses for enriching olivine Ni concentration are considered here: formation from a secondary pyroxenite source, presence of high Ni variation in mantle peridotite, formation from a deep-mantle source located near the core, or chemical diffusion. Olivines from several Hawaiian volcanoes, including Niihau, Kahoolawe, and Mauna Kea, are studied by in-situ major elemental, bulk-mineral major elemental, and bulk-mineral Mg-Fe isotopic analyses and the results are used to test the above mentioned hypotheses.

Olivines from Niihau are zoned in MgO, FeO, and NiO contents across their diameters. Comparing to basalt whole-rocks from Kauai and Niihau, olivines from Niihau plot at a steeper slope for Ni vs. MgO content. In addition, these olivines also plot at a significantly higher NiO concentration at a given Fo content compared to global olivines.

The in-situ Niihau olivine data are compared to models of fractional crystallization and chemical diffusion, with the data following the diffusion-based model for NiO vs. Fo content. This indicates that chemical diffusion likely resulted in the formation of elemental zoning, which would also indicate that the olivines were enriched in Ni at a given MgO content by this process. Assuming that olivines at Niihau underwent chemical diffusion, simplified mathematical models of diffusion were compared to approximate a timescale of 10000 days (~27 years) for diffusion within a specific olivine grain.

The isotopic data of the olivines show a strong negative correlation for Mg and Fe isotopic compositions for each study location; this is consistent with the expected fractionation trend of chemical diffusion. In addition, it can also be seen that the olivines from Niihau plot

similarly along Mg-Fe isotopic content to those of other studies interpreting chemical diffusion. Several radial and bulk diffusion models also show consistency with the Mg-Fe isotopic data. Therefore, the olivines at Niihau were enriched in Ni at given MgO content by chemical diffusion.

This study expanded the current perspective of chemical diffusion in olivine by looking at sample sets from three different ocean-island volcanic regions around Hawaii. This allowed for a comprehensive test of the findings of numerous studies. It is also seen that chemical diffusion in olivine is a widespread process, likely effecting formation of the mineral in a variety of different geologic settings. Being a new form of geochronometry, the diffusion models used here for Niihau may also be applied to estimate the timing of magmatic equilibration of olivine or other minerals from locations throughout the region.

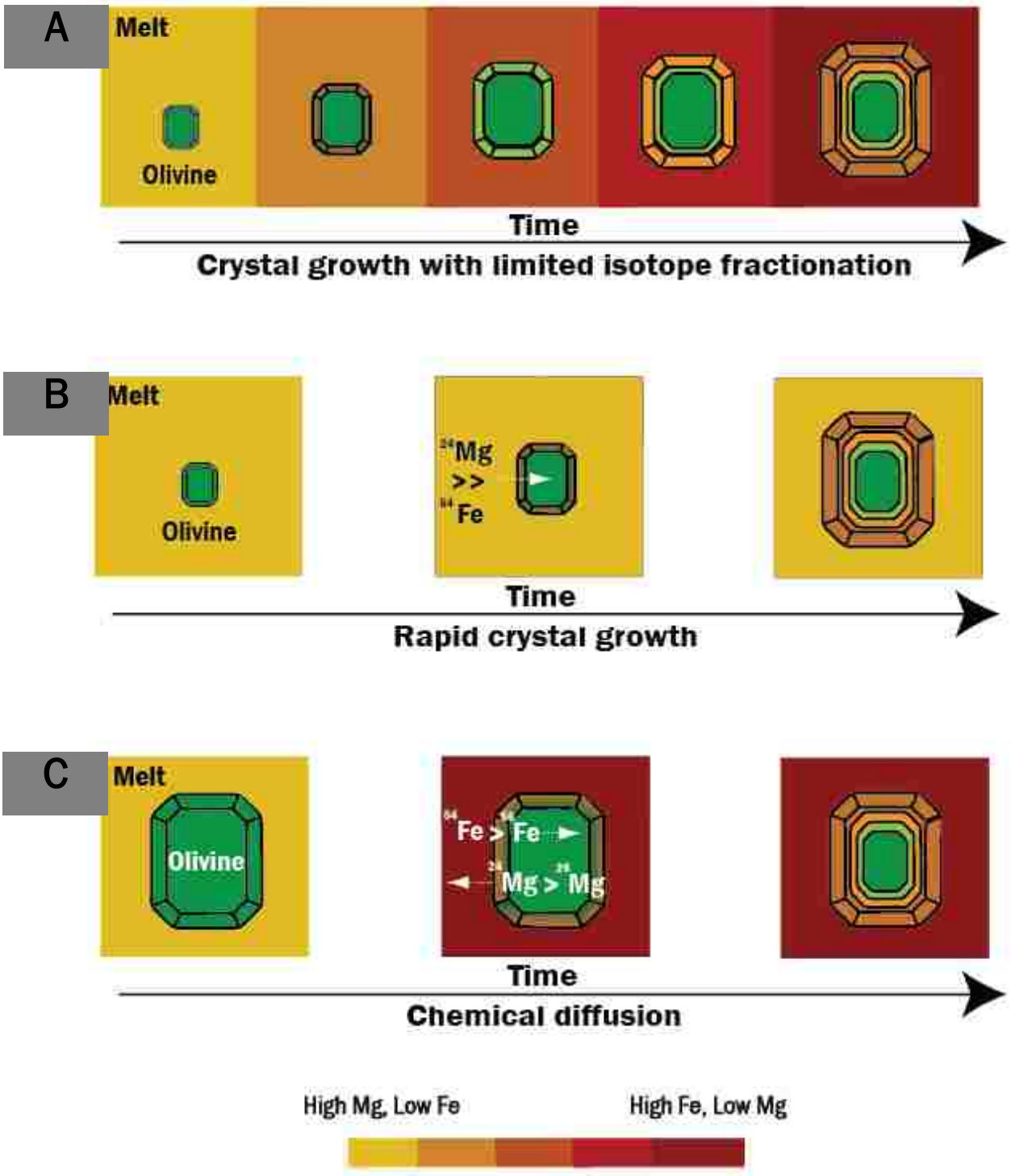

Figure 1: Forsterite elemental zoning within olivines formed by three potential processes: fractional crystallization (crystal growth with limited isotope fractionation) (**A**), rapid crystal growth (**B**), and chemical diffusion (**C**). Cartoon modified from Teng et al. (2011).

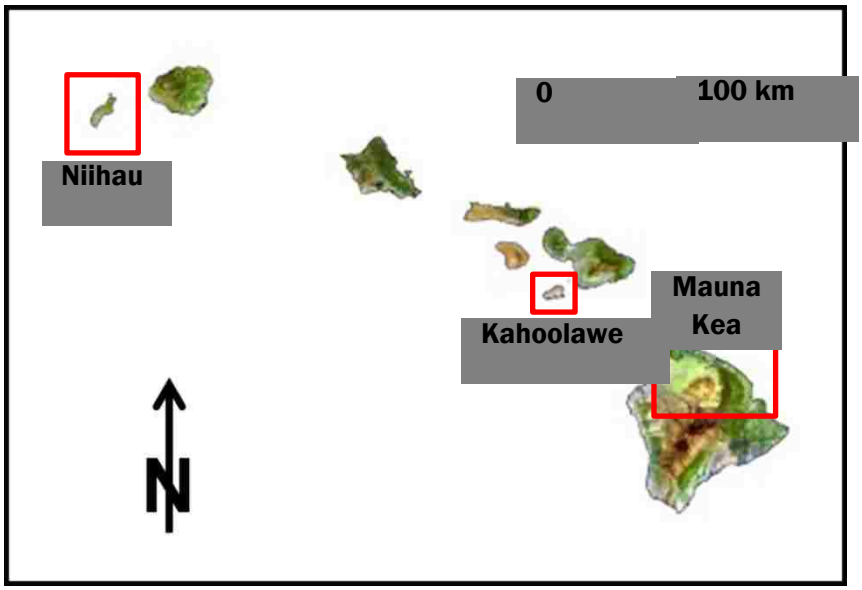

Figure 2: Map of the windward Hawaiian Islands; the locations of Niihau, Kahoolawe, and Mauna Kea are shown in red boxes. Map modified from Starr (2007).

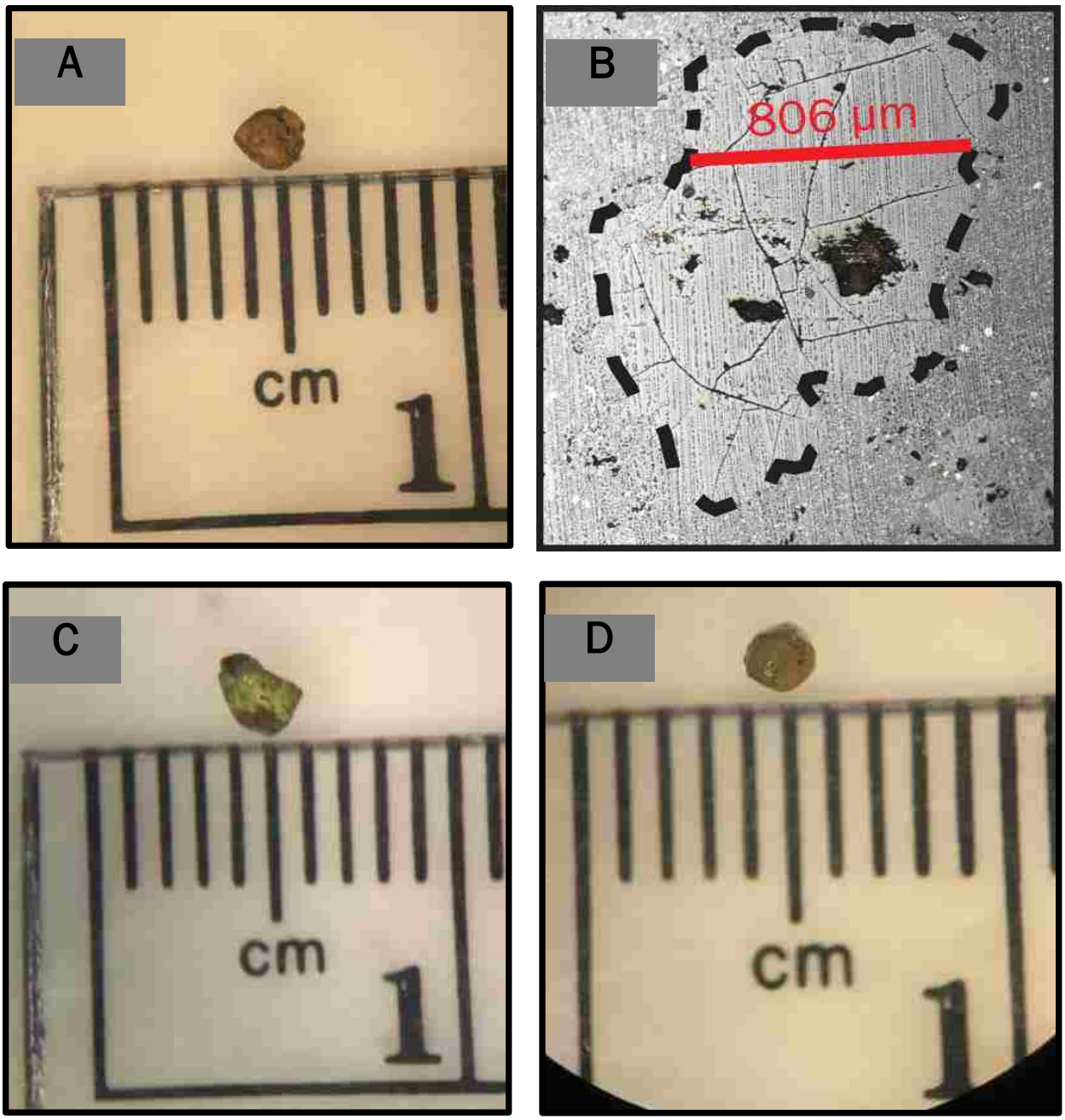

Figure 3: Four examples of olivine grains from the study locations: **A** - Niihau olivine (sample 75-Nii-4-7; not analyzed), **B** - Niihau in-situ olivine (sample 75-Nii-2-8) with 806-µm microprobe track shown, **C** - Mauna Kea olivine (sample HSDP-284-10), and **D** - Kahoolawe olivine (sample Kah-16-20).

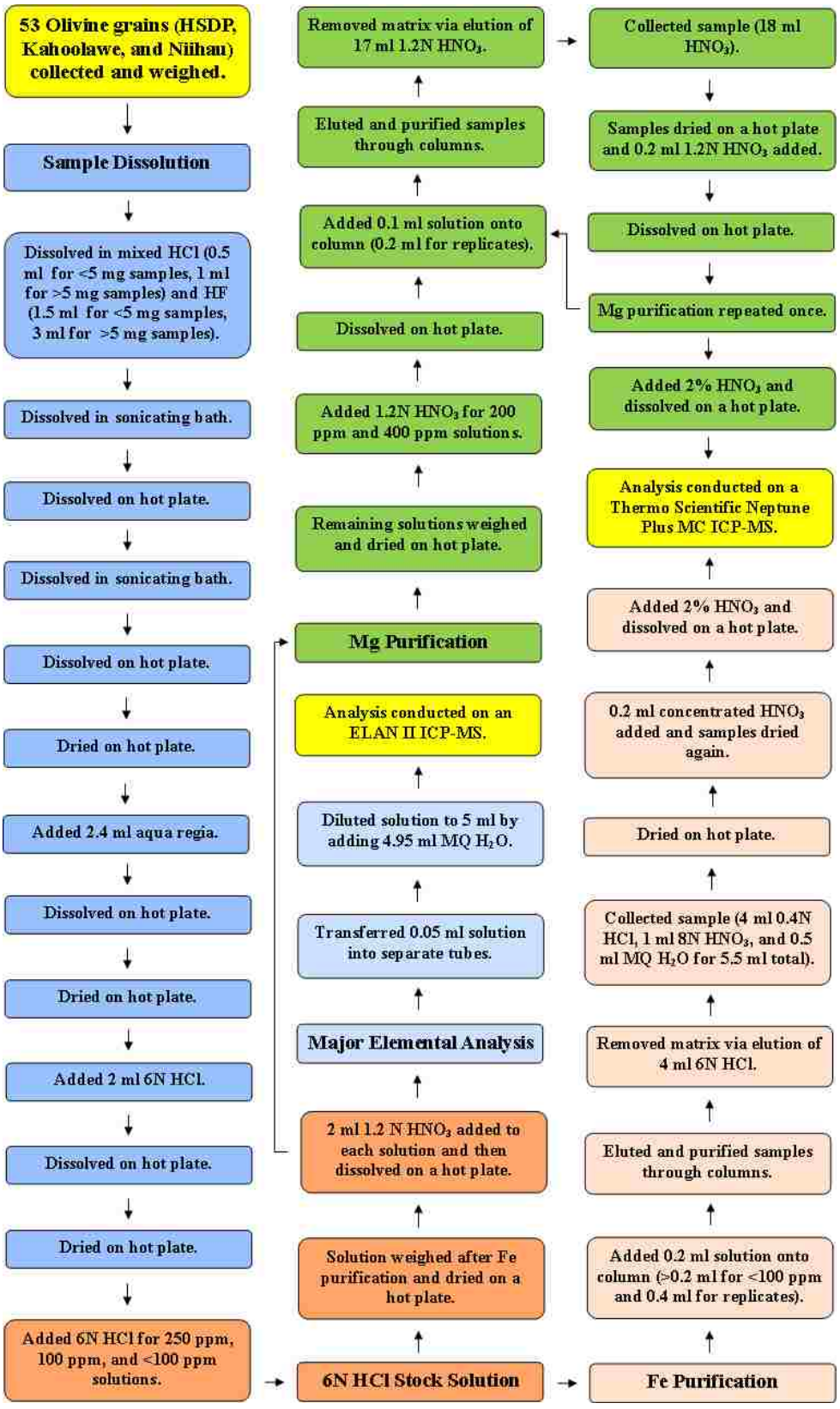

Figure 4: Flowchart of bulk olivine dissolution process, Mg-Fe purification, and analyses (begins at the top left box). Box coloring explained in text (yellow boxes refer to the initial solid olivine samples and analysis endpoints).

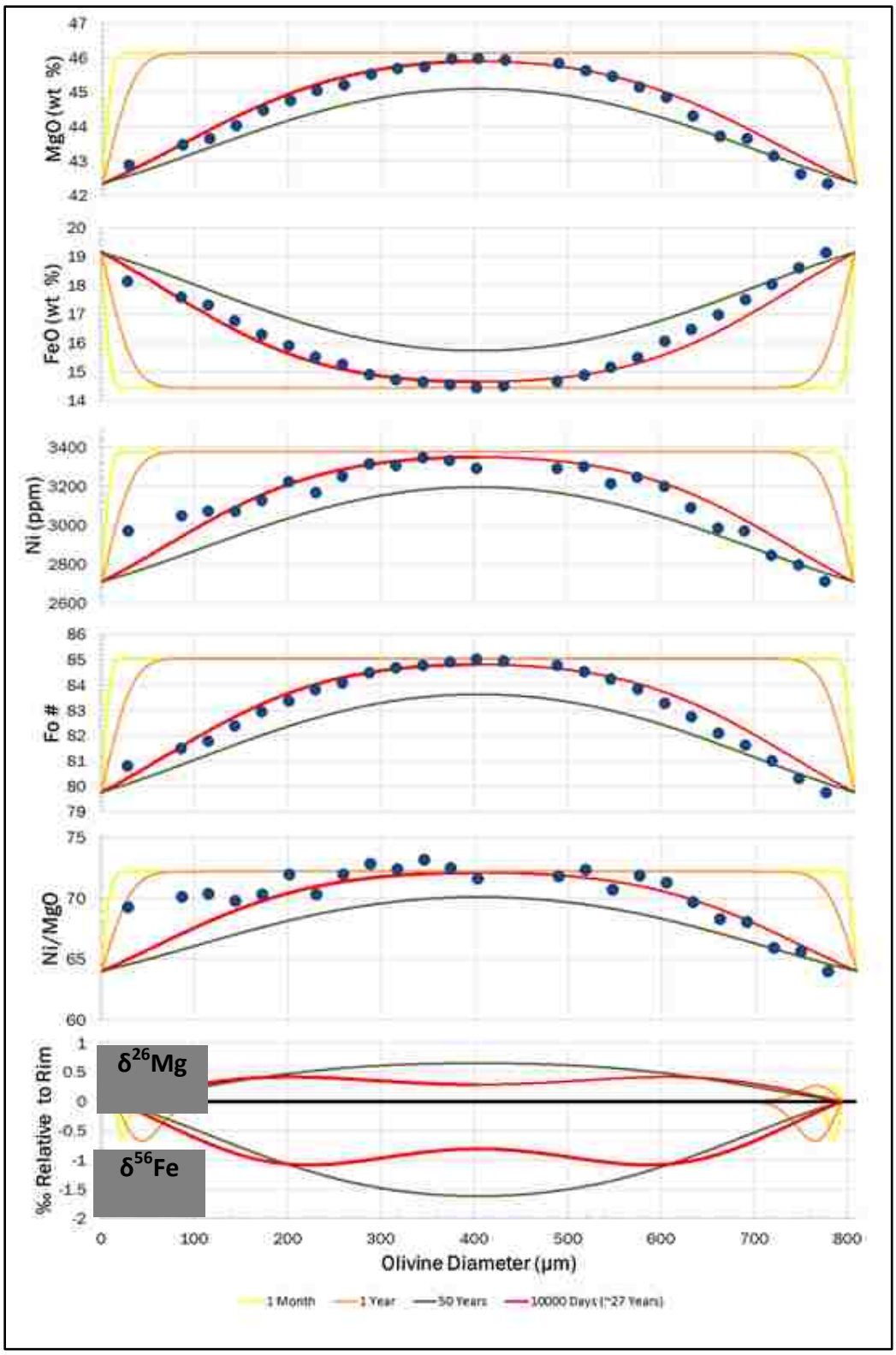

Figure 5: MgO (wt %), FeO (wt %), Ni (ppm), Fo (#), and Ni/MgO elemental profiles of one of the measured in-situ olivines (75-Nii-2-8; see **Figure 3B**), along with calculated elemental diffusion profiles and a modeled Mg-Fe isotopic diffusion profile (bottom plot). Blue points are 30-µm spot analyses. Diffusion was calculated for 1 month, 1 year, 10000 days (~27 years), and 50 years.

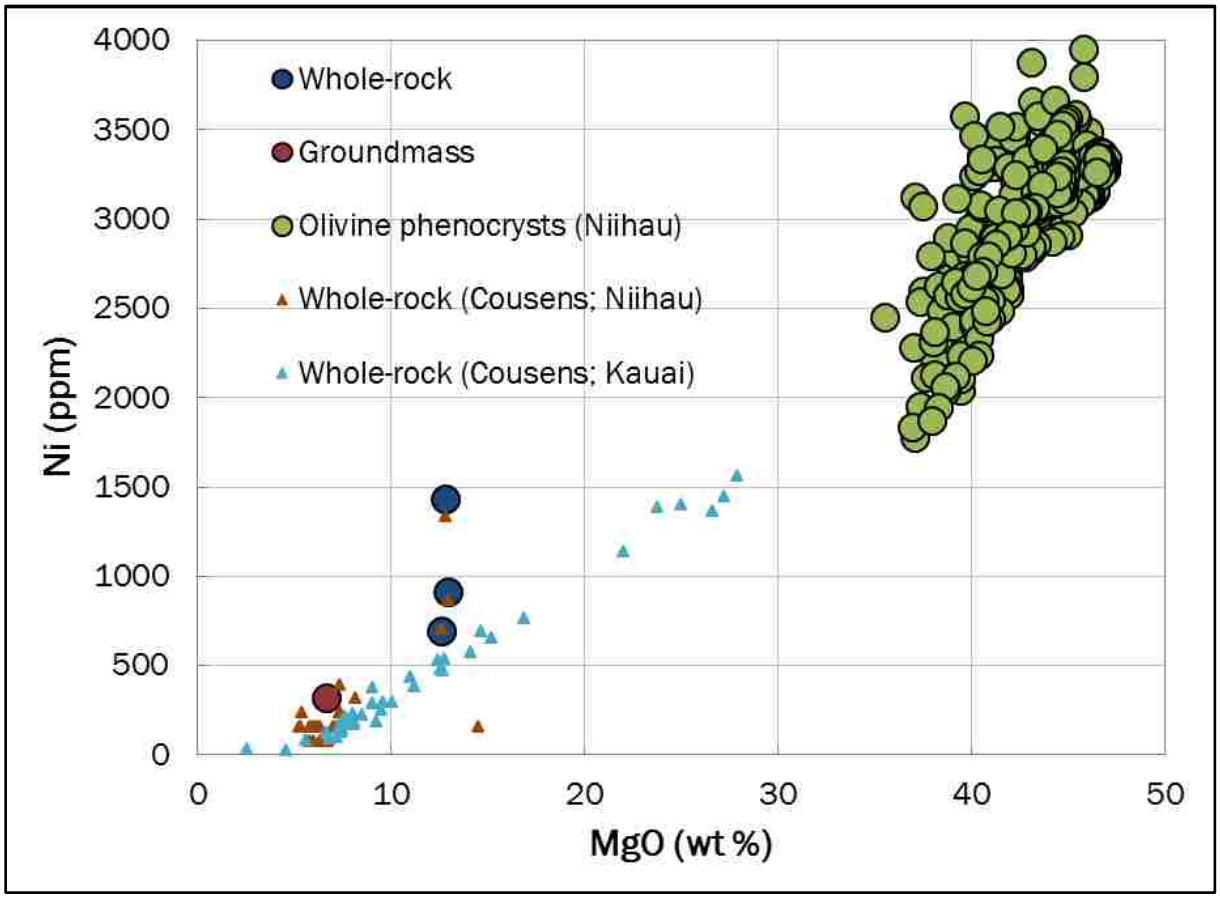

Figure 6: Plot comparing MgO (wt %) content vs. Ni (ppm) concentration for the in-situ Niihau olivines (combined spot analyses of all 13 of the phenocrysts) with the regional whole-rock data. The compositions of the three basalt whole-rocks (along with a groundmass composition) from which the olivines were derived from are shown for comparison. Regional whole-rock data is from Cousens and Clague (2015). Uncertainty is less than the size of the symbols. In-situ data are compiled in **Appendix A1**.

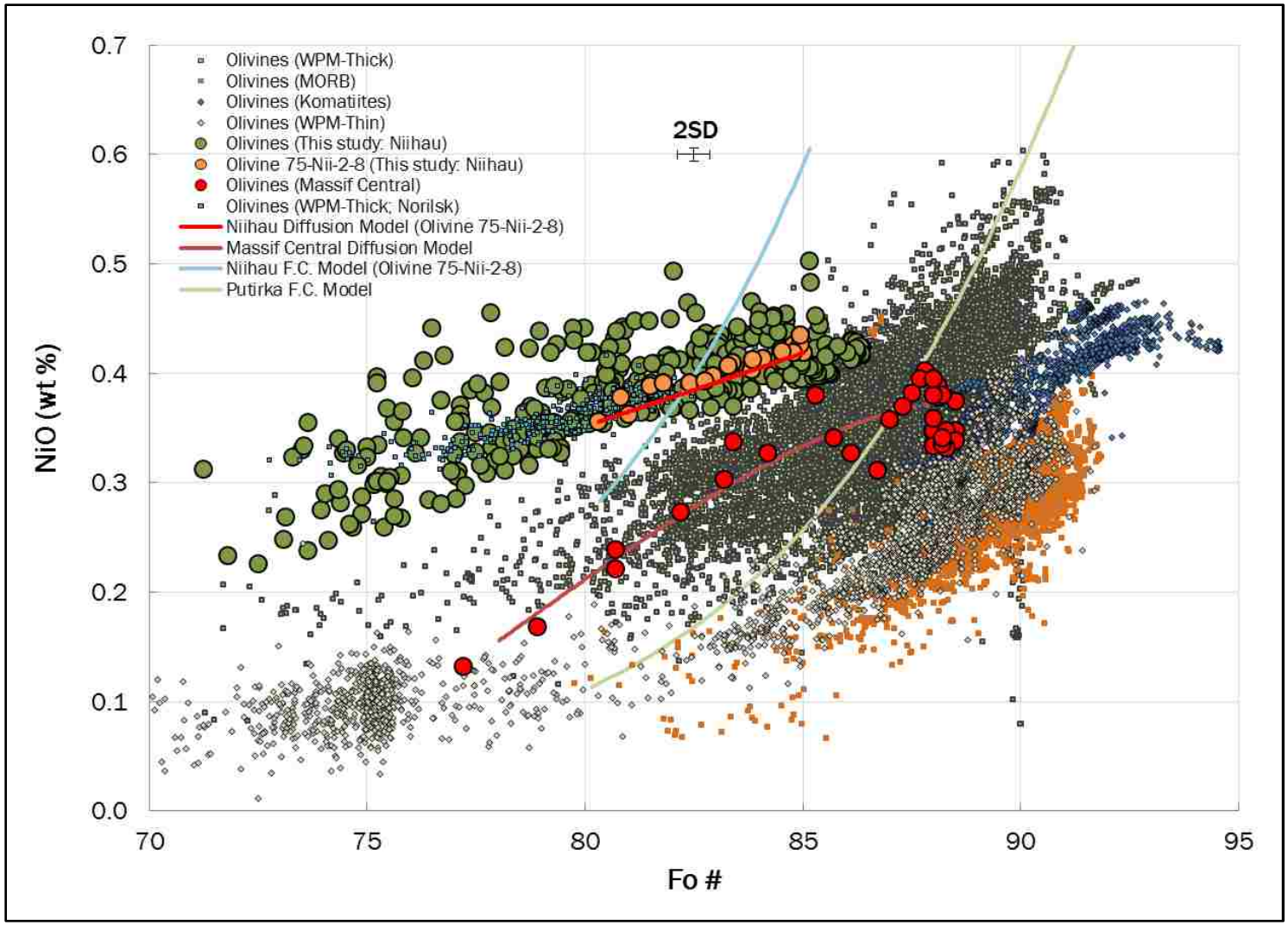

Figure 7: Global Fo (#) vs. NiO (wt %) olivine data compared to olivines from Niihau. The global data consist of olivines from MORB (mid-ocean ridge basalt), komatiites, and within plate magmas (WPM), where WPM is subdivided for magmas over thin (WPM-Thin; <70 km) and thick (WPM-Thick; >70 km) lithosphere [as in Sobolev et al. (2007)]. Models of fractional crystallization (i.e. Putirka et al., 2011) and diffusion (i.e. Crank, 1975 and Albaréde, 1996) are shown for comparison. The global data are from Sobolev et al. (2007) (including Norilsk data), Putirka et al. (2011), Oeser et al. (2015) (including Massif Central data), and Hartley et al. (2016); literature data are described in **Appendix A3**.

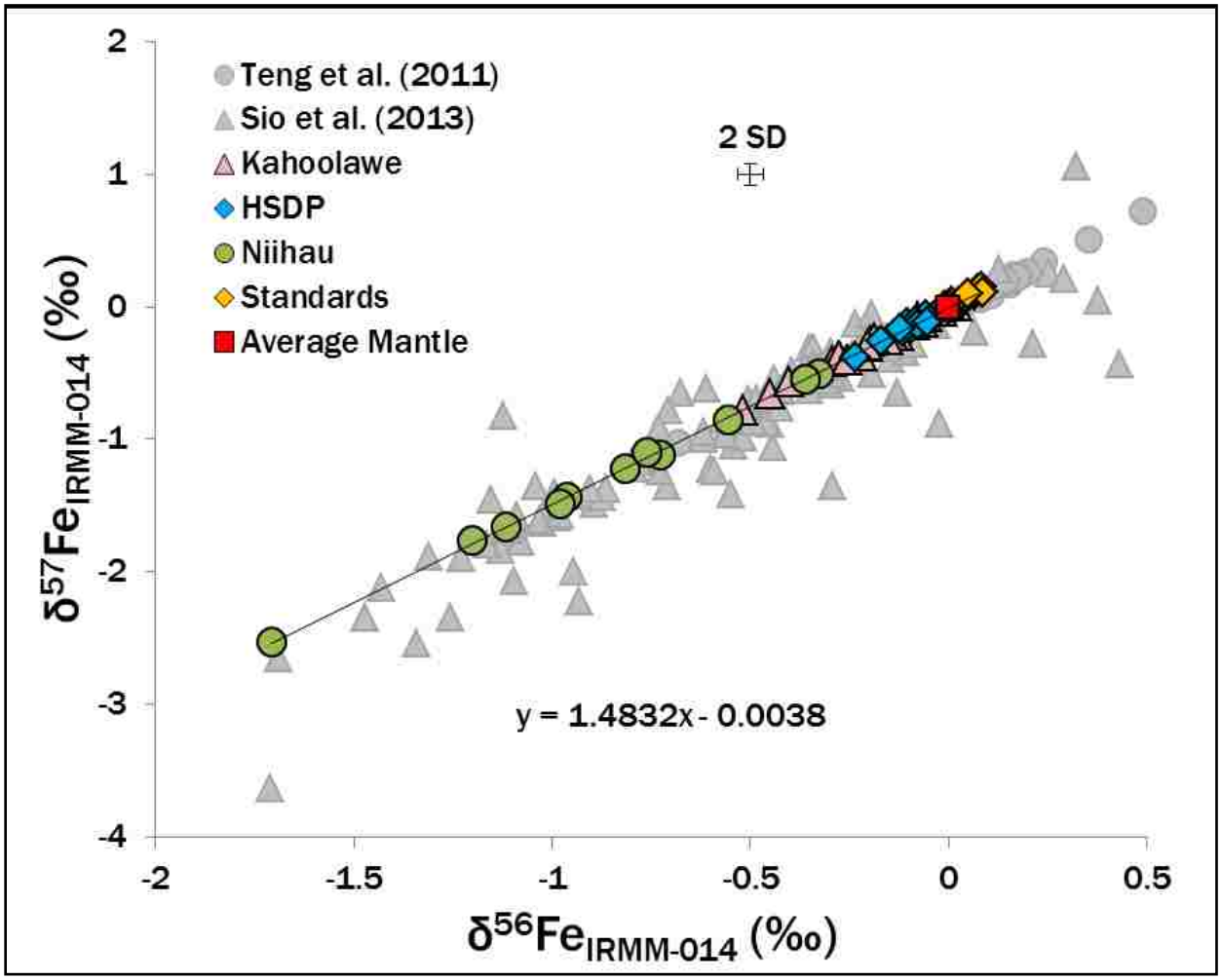

Figure 8: $\delta^{56}Fe_{IRMM-014}$ (‰) vs. $\delta^{57}Fe_{IRMM-014}$ (‰) of the olivines from the three study locations, along with olivine data from Teng et al. (2011) and Sio et al. (2013), several measured standards, and the average mantle composition [from Teng et al. (2010) and An et al. (2017)]. The olivine data forms a positive correlation, the trend being shown for comparison. Olivine and standard Fe isotopic data and information on literature data are compiled in **Appendices A2** and **A3**, respectively.

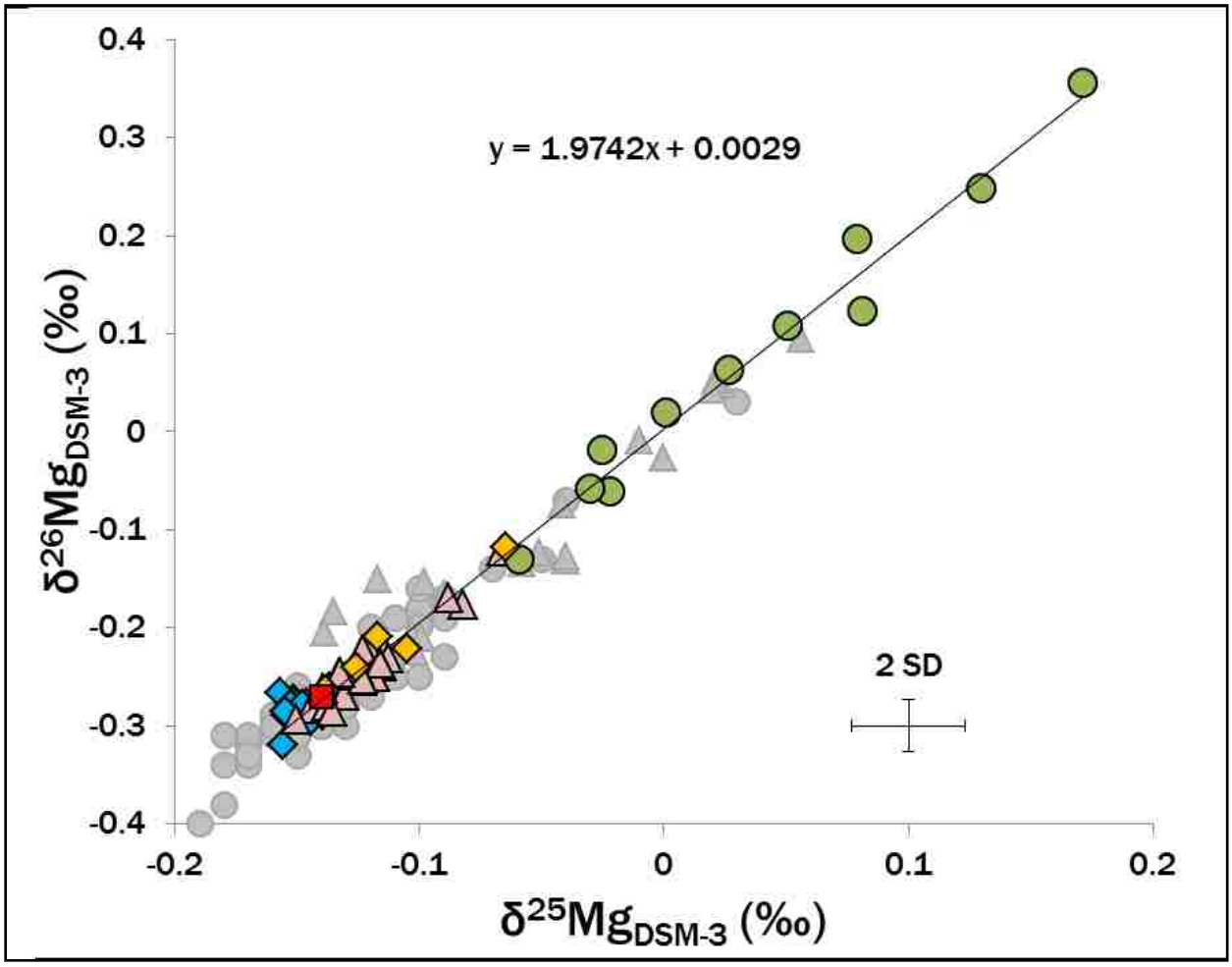

Figure 9: $\delta^{25}Mg_{DSM-3}$ (‰) vs. $\delta^{26}Mg_{DSM-3}$ (‰) of the olivines from the three study locations, along with olivine data from Teng et al. (2011) and Sio et al. (2013), several measured standards, and the average mantle composition [from Teng et al. (2010) and An et al. (2017)]. The olivine data forms a positive correlation, the trend being shown for comparison. Olivine and standard Mg isotopic data and information on literature data are compiled in **Appendices A2** and **A3**, respectively. Symbols as in **Figure 8**.

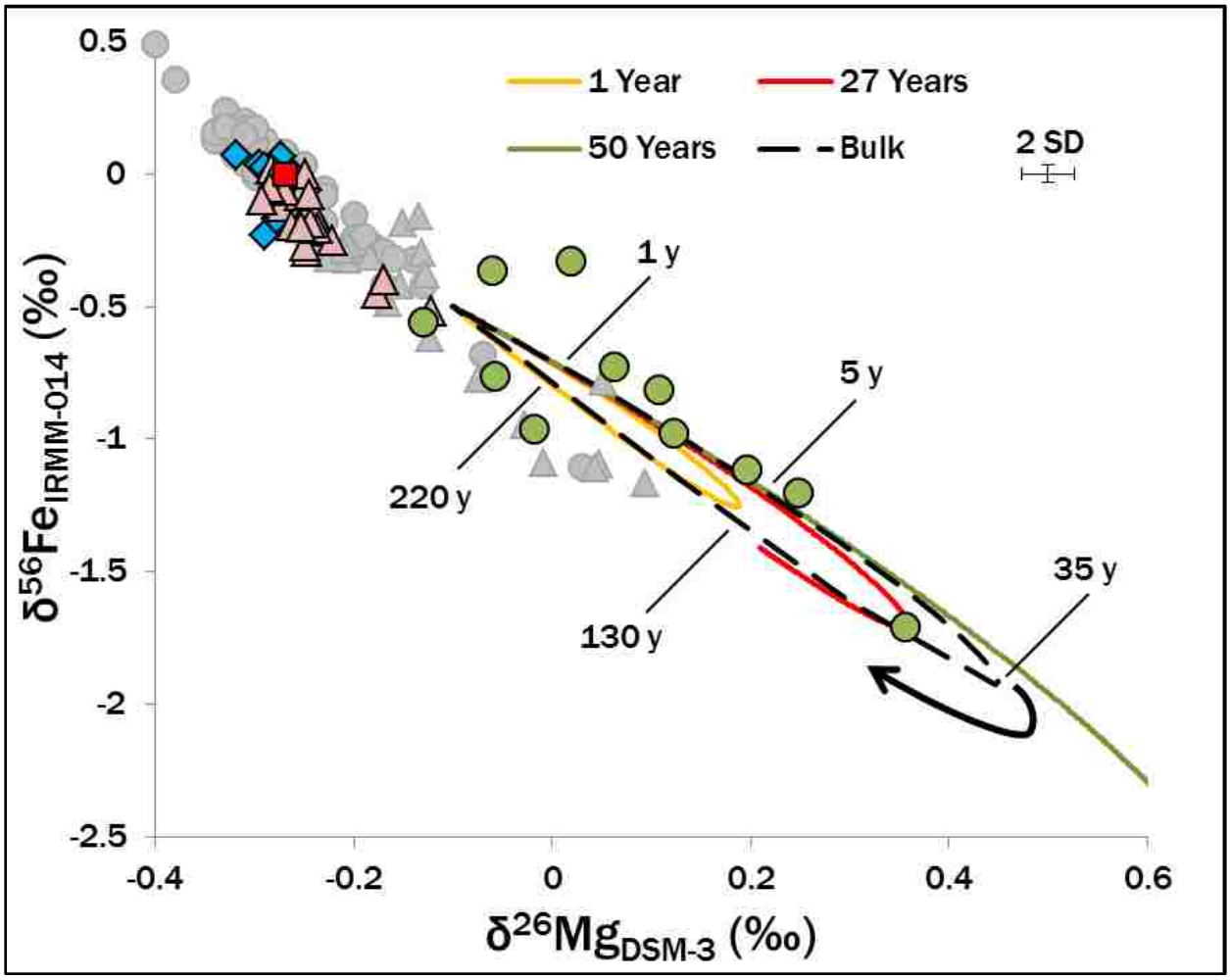

Figure 10: $\delta^{26}Mg_{DSM-3}$ (‰) vs. $\delta^{56}Fe_{IRMM-014}$ (‰) of the olivines from the three study locations, along with olivine data from Teng et al. (2011) and Sio et al. (2013) and the average mantle composition [from Teng et al. (2010) and An et al. (2017)]. The data forms a strong negative correlation, plotting along a similar trend to the samples from the two sources. Radial diffusion models of varying timescale and a bulk diffusion model calibrated to the Niihau data are plotted for comparison. The timescale for the bulk diffusion model is also plotted; after ~35 years, it is expected that the Mg-Fe isotopic composition will reverse trend, becoming less fractionated once again (following the solid black arrow). Symbols as in **Figure 8**.

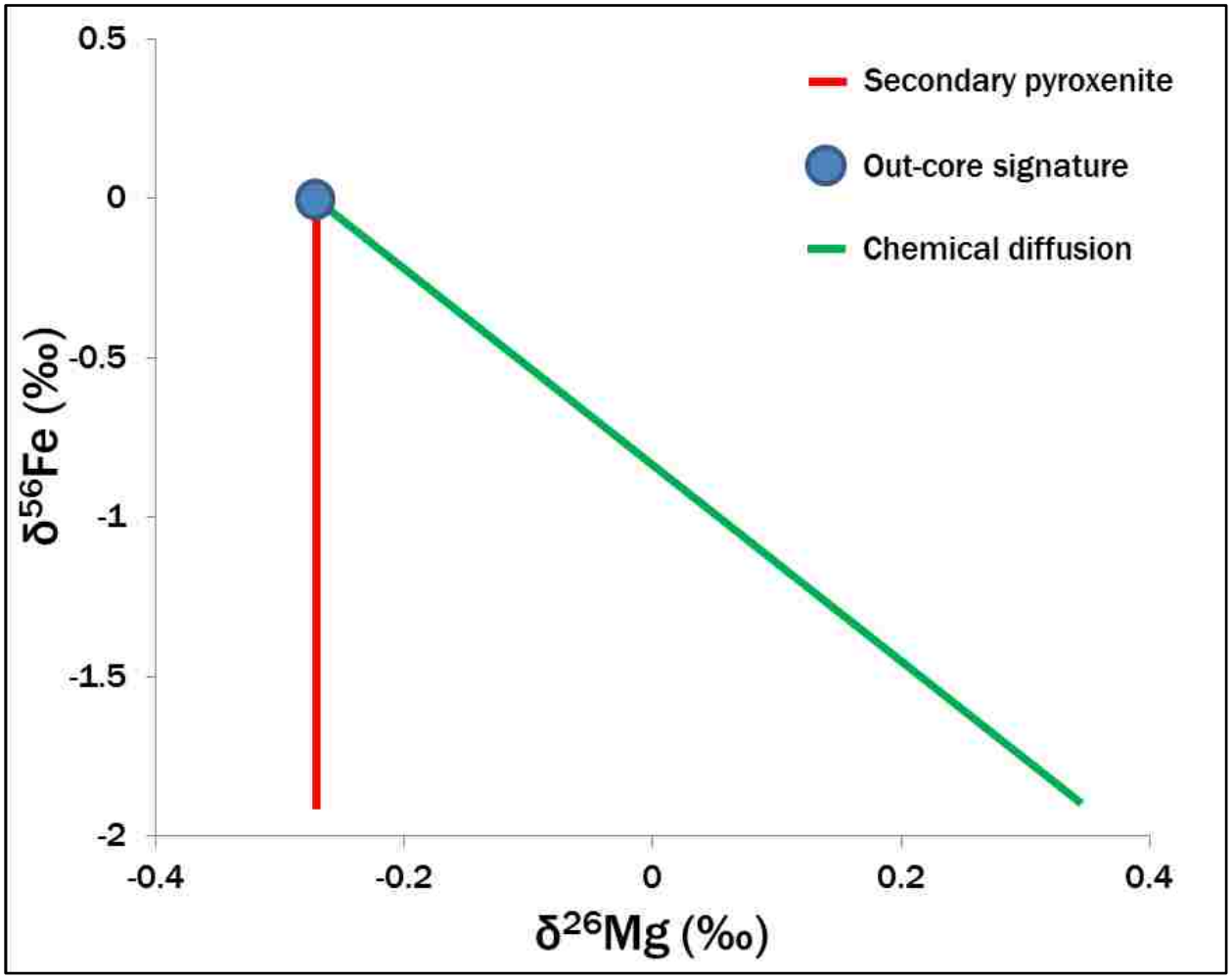

Figure 11: Hypothetical δ^{26}Mg (‰) vs. δ^{56}Fe (‰) trend for olivines enriched in Ni at a given MgO content by a secondary pyroxenite source (red line), a deep mantle source (cluster around blue circle), and chemical diffusion (green line). Olivines derived from a high Ni peridotite source as a result of mantle variation are expected to show a large degree of scatter relative to the other hypotheses.

Appendix A: Data

A1: Electron microprobe major elemental data

Table A1-1: Electron microprobe parameters for elements analyzed.

Element	Standard	2SD (%)*	Crystal (WDS)	Counting time (s)
MgO	Geller 3N Mg crystal	0.1	TAP	30
SiO_2	Geller 5N Si crystal	0.92	TAP	30
FeO	NMNH 96189 (illmenite)	0.64	LiF	30
MnO	NMNH 96189 (illmenite)	0.60	LiF	60
NiO	Synthetic Ni olivine	0.62	LiF	120

*2SD (%) calculated relative to standards NMNH 111312-44 (San Carlos olivine) and USNM 2566 (Springwater olivine).

Table A1-2: 50-μm Niihau olivine major elemental spot analyses.

Sample	Analysis No.	SiO_2 (wt %)	MgO (wt %)	FeO (wt %)	MnO (wt %)	NiO (wt %)	Fo (#)	Cations (mol)	Total (wt %)
75-Nii-1-1	11	39.3	40.1	21.4	0.25	0.37	77.1	1.96	101.6
	12	39.0	40.6	21.3	0.22	0.39	77.4	1.96	101.8
	13	39.2	39.4	21.0	0.30	0.36	77.1	1.93	100.6
	16	39.7	39.7	20.3	0.28	0.46	77.8	1.94	100.8
	17	39.2	40.5	19.0	0.25	0.43	79.4	1.93	100.3
	18	39.1	42.3	18.8	0.20	0.42	80.2	1.97	101.1
	19	39.6	42.3	18.5	0.20	0.40	80.5	1.97	101.3
	20	39.6	41.9	18.4	0.21	0.38	80.4	1.96	101.1
	21	39.7	42.3	18.0	0.16	0.44	80.9	1.97	100.7
	22	39.4	42.3	18.1	0.20	0.40	80.8	1.97	100.6
	24	39.3	42.5	18.3	0.20	0.43	80.7	1.97	101.1
	25	39.8	42.5	18.1	0.22	0.43	80.8	1.98	101.3
	26	39.7	42.4	18.2	0.20	0.37	80.7	1.97	101.2
	27	39.8	42.2	17.9	0.21	0.44	80.9	1.97	100.9
	28	39.8	42.3	18.0	0.26	0.41	80.8	1.97	101.0
	29	38.9	41.1	18.5	0.25	0.42	80.0	1.93	99.6
	30	39.8	42.0	18.7	0.26	0.39	80.1	1.97	101.4
	31	39.5	41.6	18.7	0.18	0.44	80.0	1.96	100.7
	32	39.2	41.7	19.1	0.25	0.44	79.7	1.96	100.9
	33	39.6	41.4	18.9	0.21	0.43	79.7	1.96	100.9
	34	39.4	41.5	19.3	0.21	0.38	79.5	1.96	101.0
	35	39.3	41.4	19.7	0.23	0.39	79.1	1.96	101.3
	36	39.4	41.2	19.8	0.22	0.44	79.0	1.96	101.2
	37	39.5	40.9	19.9	0.24	0.37	78.8	1.96	101.1
	38	39.6	41.3	20.1	0.22	0.42	78.7	1.97	101.8
	39	39.8	41.3	20.0	0.27	0.35	78.8	1.97	101.9

Table A1-2: Continued.

Sample	Analysis No.	SiO_2 (wt %)	MgO (wt %)	FeO (wt %)	MnO (wt %)	NiO (wt %)	Fo (#)	Cations (mol)	Total (wt %)
	40	39.5	40.7	20.2	0.25	0.35	78.4	1.96	101.3
	41	39.1	40.8	20.0	0.28	0.36	78.6	1.95	100.8
	44	39.1	40.4	20.9	0.28	0.38	77.7	1.95	101.2
	45	38.7	37.1	22.0	0.34	0.40	75.2	1.88	99.3
	46	39.4	37.5	22.2	0.33	0.39	75.2	1.91	100.5
	47	39.3	39.8	21.2	0.26	0.36	77.2	1.95	101.3
	48	39.2	40.5	21.2	0.33	0.35	77.5	1.96	101.8
	49	38.8	40.5	20.9	0.26	0.31	77.7	1.95	101.0
75-Nii-1-2	1	38.2	38.3	23.8	0.26	0.29	74.3	1.92	101.2
	2	38.5	38.9	23.3	0.29	0.33	75.0	1.94	101.6
	3	38.9	38.8	22.7	0.25	0.37	75.5	1.93	101.3
	4	39.2	39.9	21.8	0.29	0.38	76.7	1.96	101.8
	5	39.6	40.5	21.1	0.29	0.39	77.5	1.97	102.1
	6	39.3	40.4	20.5	0.18	0.39	78.0	1.95	101.0
	7	39.4	41.2	19.7	0.18	0.36	79.0	1.96	101.1
	8	39.2	41.6	19.2	0.17	0.35	79.6	1.96	100.8
	9	39.7	42.1	18.4	0.20	0.39	80.4	1.97	101.0
	10	39.7	42.2	18.1	0.19	0.44	80.7	1.97	100.8
	11	39.9	42.3	17.7	0.18	0.45	81.1	1.97	100.9
	12	39.7	42.7	17.5	0.15	0.37	81.4	1.97	100.8
	13	39.6	42.9	17.0	0.20	0.42	81.9	1.97	100.4
	14	40.6	43.7	17.3	0.18	0.45	82.0	2.01	102.5
	15	39.7	43.1	17.0	0.20	0.49	82.0	1.98	100.7
	16	39.7	43.2	16.6	0.23	0.47	82.4	1.97	100.5
	17	39.1	43.3	16.6	0.18	0.39	82.5	1.96	99.7

Table A1-2: Continued.

Sample	Analysis No.	SiO_2 (wt %)	MgO (wt %)	FeO (wt %)	MnO (wt %)	NiO (wt %)	Fo (#)	Cations (mol)	Total (wt %)
	18	39.4	43.2	16.7	0.15	0.41	82.4	1.97	100.1
	19	39.8	43.5	16.6	0.21	0.46	82.5	1.98	100.7
	20	39.3	43.5	16.4	0.15	0.41	82.7	1.97	100.1
	21	39.4	43.0	16.3	0.19	0.43	82.6	1.96	99.6
	29	40.4	45.1	14.8	0.14	0.45	84.6	2.01	101.1
	30	40.2	44.3	15.4	0.18	0.47	83.8	1.99	100.8
	31	39.9	43.6	16.2	0.20	0.41	82.9	1.98	100.6
	32	39.0	41.5	17.0	0.21	0.45	81.5	1.92	98.7
	36	39.3	40.0	21.5	0.26	0.36	77.0	1.95	101.7
	37	38.8	38.9	22.4	0.24	0.31	75.8	1.93	101.0
	38	38.8	38.3	23.6	0.26	0.33	74.5	1.93	101.5
	39	39.1	38.1	23.6	0.32	0.28	74.4	1.93	101.7
	40	38.7	37.5	24.3	0.34	0.33	73.5	1.92	101.4
	41	38.8	37.4	24.5	0.34	0.32	73.3	1.92	101.7
	42	38.6	37.3	24.8	0.35	0.25	73.1	1.92	101.5
75-Nii-1-3	6	38.4	37.1	25.3	0.31	0.23	72.5	1.92	101.6
	9	38.5	35.5	25.8	0.28	0.31	71.2	1.89	100.7
	12	38.9	38.2	24.2	0.24	0.28	74.0	1.94	102.2
	13	38.8	38.8	24.1	0.31	0.34	74.3	1.95	102.8
	15	38.7	38.4	23.7	0.28	0.33	74.5	1.94	101.7
	17	38.9	39.2	23.2	0.29	0.34	75.2	1.95	102.1
	18	38.9	38.8	23.4	0.31	0.29	74.9	1.94	102.0
	19	38.9	39.2	23.1	0.33	0.31	75.3	1.95	102.1
	21	38.9	39.2	23.3	0.28	0.30	75.2	1.95	102.3
	22	38.9	39.3	23.4	0.29	0.30	75.2	1.96	102.4

Table A1-2: Continued.

Sample	Analysis No.	SiO_2 (wt %)	MgO (wt %)	FeO (wt %)	MnO (wt %)	NiO (wt %)	Fo (#)	Cations (mol)	Total (wt %)
	24	38.9	39.3	23.0	0.23	0.30	75.4	1.95	102.0
	25	38.9	39.1	23.2	0.29	0.30	75.2	1.95	102.0
	26	38.9	39.2	22.8	0.32	0.36	75.6	1.95	101.8
75-Nii-1-4	2	38.6	37.0	26.1	0.29	0.23	71.8	1.93	102.5
	4	38.5	37.6	24.9	0.31	0.27	73.1	1.93	101.8
	5	38.5	38.3	24.8	0.29	0.33	73.6	1.94	102.4
	6	38.8	37.9	24.4	0.29	0.36	73.6	1.93	102.0
	8	39.3	39.4	23.6	0.27	0.32	75.0	1.97	103.2
	9	37.8	37.0	23.4	0.29	0.29	74.0	1.88	100.2
	10	39.1	38.0	23.6	0.23	0.29	74.3	1.93	101.5
	12	39.0	39.7	22.8	0.31	0.37	75.8	1.96	102.2
	13	39.2	39.7	22.8	0.27	0.34	75.8	1.96	102.4
	14	39.1	40.1	22.4	0.24	0.41	76.3	1.97	102.5
	15	39.2	40.4	22.0	0.27	0.42	76.8	1.97	102.5
	16	39.0	39.3	22.3	0.26	0.40	76.0	1.94	101.6
	18	39.3	40.1	22.2	0.25	0.44	76.5	1.97	102.6
	19	38.9	40.0	22.5	0.25	0.34	76.2	1.96	102.2
	21	39.1	38.4	23.3	0.25	0.32	74.8	1.94	101.7
	23	38.1	39.1	22.8	0.28	0.31	75.5	1.93	100.8
	24	39.2	40.1	22.3	0.22	0.28	76.4	1.96	102.3
	26	39.2	41.2	21.1	0.24	0.37	77.9	1.98	102.3
	27	39.5	41.9	19.8	0.21	0.42	79.2	1.98	102.1
	28	39.0	41.3	17.9	0.30	0.37	80.6	1.93	99.4
	29	40.0	43.6	17.4	0.23	0.42	81.9	2.00	101.9
	30	40.2	44.9	16.0	0.20	0.39	83.5	2.01	101.9

Table A1-2: Continued.

Sample	Analysis No.	SiO_2 (wt %)	MgO (wt %)	FeO (wt %)	MnO (wt %)	NiO (wt %)	Fo (#)	Cations (mol)	Total (wt %)
	31	40.3	45.3	14.8	0.22	0.45	84.6	2.01	101.4
	32	40.4	45.8	14.4	0.14	0.50	85.1	2.02	101.4
	33	40.5	45.7	14.2	0.15	0.44	85.3	2.01	101.3
	34	40.5	46.1	14.2	0.16	0.44	85.4	2.02	101.7
	35	40.3	45.5	14.1	0.15	0.45	85.3	2.00	100.9
	36	40.3	45.9	14.4	0.15	0.48	85.2	2.02	101.6
	37	40.0	44.8	14.6	0.18	0.44	84.7	1.99	101.3
	38	40.2	45.5	15.2	0.19	0.42	84.4	2.02	101.7
	39	40.0	45.4	15.6	0.20	0.46	84.0	2.02	101.8
	40	39.9	44.2	16.6	0.17	0.40	82.7	2.00	101.5
	41	40.0	42.8	18.6	0.21	0.42	80.6	2.00	102.3
	42	39.7	40.6	20.4	0.22	0.42	78.2	1.96	101.6
Average									
75-Nii-1-1		39.4	41.1	19.6	0.24	0.40	79.0	1.96	101.0
75-Nii-1-2		39.4	41.3	19.5	0.22	0.39	79.2	1.96	100.9
75-Nii-1-3		38.8	38.6	23.7	0.29	0.30	74.5	1.95	102.0
75-Nii-1-4		39.4	41.6	19.9	0.23	0.38	78.9	1.97	101.8
Whole-rocks									
75-Nii-1		-	12.93	-	-	0.11	-	-	-
75-Nii-2		-	12.81	-	-	0.17	-	-	-
75-Nii-4		-	12.61	-	-	0.09	-	-	-
75-Nii-1 groundmass		51.0	6.7	7.1	0.10	0.04	62.9	-	98.8

Table A1-3: 30-µm Niihau olivine major elemental spot analyses.

Sample	Analysis No.	SiO_2 (wt %)	MgO (wt %)	FeO (wt %)	MnO (wt %)	NiO (wt %)	Fo (#)	Cations (mol)	Total (wt %)
75-Nii-2-1	2	38.6	39.2	20.7	0.24	0.34	77.1	1.91	99.5
	3	38.3	39.7	20.6	0.24	0.33	77.5	1.92	99.4
	4	38.1	40.0	20.3	0.23	0.33	77.9	1.92	99.2
	6	38.6	40.5	19.2	0.21	0.36	79.0	1.92	99.1
	8	38.8	41.8	17.9	0.19	0.37	80.6	1.94	99.3
	9	39.0	42.3	17.4	0.17	0.38	81.3	1.95	99.5
	11	38.8	42.7	16.3	0.17	0.39	82.4	1.94	98.6
	13	39.2	43.6	15.4	0.15	0.40	83.4	1.96	99.1
	14	39.3	43.9	15.2	0.16	0.39	83.7	1.96	99.3
	15	39.3	44.2	14.9	0.14	0.40	84.1	1.97	99.3
	16	39.4	44.2	14.7	0.15	0.40	84.3	1.96	99.0
	17	39.5	44.4	14.5	0.14	0.40	84.5	1.97	99.2
	18	39.4	44.4	14.3	0.14	0.41	84.7	1.96	99.0
	19	39.4	44.4	14.2	0.14	0.40	84.8	1.96	98.9
	20	39.3	44.4	14.2	0.14	0.39	84.8	1.96	98.7
	22	39.4	44.6	14.1	0.14	0.41	85.0	1.97	98.9
	23	39.3	44.7	14.0	0.13	0.40	85.0	1.97	98.7
	24	39.6	44.7	14.1	0.14	0.41	85.0	1.97	99.2
	25	39.5	44.6	14.0	0.14	0.41	85.0	1.97	98.9
	26	39.5	44.7	14.0	0.13	0.40	85.0	1.97	99.0
	27	39.5	44.6	13.9	0.14	0.41	85.1	1.96	98.9
	28	39.7	44.8	13.9	0.15	0.40	85.1	1.97	99.3
	29	39.5	44.8	14.0	0.14	0.42	85.1	1.97	99.1
	31	39.6	44.8	14.0	0.14	0.41	85.1	1.97	99.2
	32	39.4	44.8	14.0	0.13	0.41	85.1	1.97	99.0
	38	39.4	44.7	13.9	0.14	0.41	85.2	1.97	98.9

Table A1-3: Continued.

Sample	Analysis No.	SiO_2 (wt %)	MgO (wt %)	FeO (wt %)	MnO (wt %)	NiO (wt %)	Fo (#)	Cations (mol)	Total (wt %)
	39	39.6	44.8	14.0	0.14	0.41	85.1	1.97	99.1
	40	39.5	44.7	14.0	0.13	0.40	85.1	1.97	99.0
	41	39.4	44.8	14.0	0.14	0.40	85.1	1.97	99.0
	42	39.6	44.9	14.0	0.14	0.41	85.1	1.98	99.3
	43	39.5	44.6	14.0	0.14	0.41	85.0	1.97	98.9
	44	39.5	44.6	14.0	0.14	0.42	85.1	1.97	99.0
	45	39.4	44.7	13.9	0.13	0.41	85.1	1.97	98.8
	46	39.5	44.7	14.0	0.15	0.41	85.1	1.97	99.0
	47	39.5	44.7	14.0	0.13	0.41	85.0	1.97	99.0
	48	39.4	44.7	13.9	0.15	0.42	85.1	1.97	98.8
	49	39.5	44.6	14.0	0.14	0.41	85.1	1.97	98.9
	50	39.4	44.7	14.0	0.14	0.40	85.1	1.97	98.8
	51	39.6	44.8	14.0	0.14	0.40	85.1	1.97	99.1
	52	39.6	44.7	13.9	0.15	0.41	85.1	1.97	99.1
	53	39.4	44.6	14.0	0.14	0.40	85.0	1.96	98.8
	54	39.5	44.6	13.9	0.14	0.41	85.1	1.96	98.8
	56	39.4	44.7	14.0	0.14	0.40	85.0	1.97	98.9
	57	39.5	44.7	14.0	0.14	0.41	85.1	1.97	99.0
	58	39.4	44.7	14.0	0.13	0.41	85.0	1.97	98.9
	59	39.6	44.7	14.0	0.14	0.41	85.0	1.97	99.1
	60	39.5	44.6	14.0	0.15	0.40	85.0	1.97	98.9
	61	39.5	44.6	14.1	0.14	0.40	85.0	1.97	99.0
	62	39.6	44.6	14.1	0.14	0.41	84.9	1.97	99.2
	63	39.5	44.6	14.3	0.14	0.40	84.8	1.97	99.1
	64	39.4	44.5	14.4	0.14	0.40	84.6	1.97	99.0
	65	39.5	44.5	14.6	0.15	0.41	84.4	1.97	99.4

Table A1-3: Continued.

Sample	Analysis No.	SiO_2 (wt %)	MgO (wt %)	FeO (wt %)	MnO (wt %)	NiO (wt %)	Fo (#)	Cations (mol)	Total (wt %)
	67	39.1	43.7	15.2	0.15	0.41	83.7	1.95	98.8
	68	39.2	43.3	15.5	0.17	0.39	83.2	1.95	99.1
	69	39.2	42.9	16.0	0.16	0.39	82.7	1.95	99.2
	70	39.1	42.8	16.5	0.18	0.39	82.2	1.95	99.1
	71	39.0	42.3	17.1	0.18	0.39	81.5	1.94	99.2
	72	38.8	41.9	17.8	0.20	0.37	80.8	1.94	99.3
	73	38.8	41.3	18.4	0.20	0.36	80.0	1.93	99.4
	74	38.7	40.9	19.0	0.22	0.36	79.3	1.93	99.4
	75	38.7	40.6	19.7	0.23	0.34	78.6	1.93	99.8
	76	38.7	40.3	20.2	0.23	0.34	78.1	1.93	100.0
75-Nii-2-2	1	38.3	38.1	22.8	0.27	0.27	74.9	1.91	99.9
	2	38.4	38.1	22.1	0.26	0.30	75.5	1.90	99.5
	3	38.3	38.8	21.7	0.26	0.33	76.1	1.91	99.7
	4	38.5	39.4	21.0	0.24	0.33	77.0	1.92	99.6
	6	38.7	40.6	19.3	0.21	0.35	79.0	1.93	99.4
	7	38.8	41.1	18.5	0.20	0.35	79.8	1.93	99.2
	9	39.1	42.5	17.2	0.18	0.37	81.5	1.95	99.8
	10	39.2	42.4	16.5	0.17	0.37	82.1	1.94	99.2
	12	39.4	43.4	15.9	0.17	0.39	83.0	1.96	99.6
	13	39.3	43.4	15.7	0.17	0.39	83.1	1.96	99.3
	14	39.4	43.5	15.6	0.16	0.38	83.3	1.96	99.3
	15	39.4	42.9	15.4	0.16	0.39	83.2	1.94	99.2
	16	39.3	43.4	15.4	0.16	0.38	83.4	1.95	99.0
	17	39.3	43.4	15.4	0.16	0.40	83.4	1.95	99.0
	19	39.7	43.8	15.4	0.17	0.40	83.5	1.97	99.8

Table A1-3: Continued.

Sample	Analysis No.	SiO_2 (wt %)	MgO (wt %)	FeO (wt %)	MnO (wt %)	NiO (wt %)	Fo (#)	Cations (mol)	Total (wt %)
	20	39.5	43.7	15.4	0.16	0.39	83.5	1.96	99.4
	21	39.3	43.6	15.4	0.16	0.39	83.4	1.96	99.1
	22	39.3	43.6	15.3	0.16	0.40	83.5	1.96	99.1
	23	39.5	43.8	15.3	0.16	0.39	83.6	1.96	99.5
	24	39.4	43.7	15.3	0.17	0.40	83.6	1.96	99.2
	26	39.3	43.6	15.3	0.16	0.40	83.5	1.96	99.1
	27	39.5	43.7	15.4	0.17	0.40	83.5	1.96	99.4
	28	39.4	43.7	15.4	0.17	0.40	83.5	1.96	99.3
	29	39.4	43.7	15.4	0.16	0.38	83.5	1.96	99.3
	30	39.4	43.6	15.4	0.17	0.38	83.4	1.96	99.3
	31	39.4	43.5	15.4	0.17	0.39	83.4	1.96	99.1
	32	39.3	43.5	15.4	0.16	0.39	83.4	1.96	99.1
	33	39.2	43.5	15.3	0.16	0.40	83.5	1.95	98.9
	37	39.2	43.4	15.3	0.16	0.41	83.5	1.95	98.8
	39	39.2	43.9	15.3	0.15	0.39	83.6	1.96	99.1
	41	39.6	43.9	15.4	0.16	0.40	83.6	1.97	99.6
	42	39.4	43.6	15.4	0.16	0.40	83.4	1.96	99.2
	43	39.4	43.8	15.5	0.17	0.38	83.4	1.97	99.5
	44	39.4	43.6	15.6	0.18	0.39	83.3	1.96	99.4
	45	39.4	43.5	15.7	0.17	0.39	83.2	1.96	99.4
	46	39.3	43.2	16.0	0.17	0.39	82.8	1.96	99.3
	47	39.3	42.9	16.4	0.18	0.38	82.3	1.95	99.5
	48	38.9	42.6	16.8	0.18	0.37	81.9	1.95	99.0
	49	38.9	42.1	17.4	0.19	0.38	81.1	1.94	99.3
	50	38.9	41.6	17.9	0.20	0.37	80.5	1.94	99.2
	51	38.7	41.0	18.6	0.21	0.36	79.7	1.93	99.2

Table A1-3: Continued.

Sample	Analysis No.	SiO_2 (wt %)	MgO (wt %)	FeO (wt %)	MnO (wt %)	NiO (wt %)	Fo (#)	Cations (mol)	Total (wt %)
	53	38.6	40.4	19.6	0.23	0.33	78.6	1.93	99.4
75-Nii-2-3	1	39.1	40.2	21.3	0.24	0.31	77.1	1.95	101.3
	2	39.0	40.6	20.5	0.23	0.34	77.9	1.95	100.9
	3	39.4	41.2	19.7	0.22	0.37	78.8	1.96	101.2
	4	39.5	41.9	19.1	0.21	0.39	79.6	1.97	101.3
	5	39.5	42.3	18.6	0.21	0.38	80.2	1.97	101.2
	6	39.4	42.4	18.4	0.20	0.38	80.4	1.97	101.1
	7	39.8	42.8	18.2	0.19	0.38	80.7	1.99	101.6
	8	39.5	42.6	18.2	0.20	0.39	80.7	1.98	101.1
	9	39.6	42.6	18.3	0.21	0.39	80.6	1.98	101.3
	10	39.7	42.7	18.3	0.20	0.38	80.6	1.98	101.5
	11	39.7	42.8	18.4	0.20	0.39	80.6	1.99	101.6
	12	39.5	42.6	18.4	0.20	0.38	80.5	1.98	101.3
	13	39.6	42.5	18.5	0.20	0.39	80.4	1.98	101.4
	14	39.6	42.9	18.3	0.20	0.38	80.6	1.99	101.6
	15	39.8	42.7	18.4	0.20	0.39	80.5	1.99	101.7
	16	39.8	42.8	18.3	0.20	0.38	80.6	1.99	101.7
	17	39.6	43.0	18.2	0.20	0.37	80.8	1.99	101.6
	18	39.8	43.1	17.9	0.20	0.39	81.1	1.99	101.7
	19	39.9	43.3	17.8	0.19	0.39	81.2	1.99	101.8
	20	39.9	43.3	17.7	0.19	0.39	81.3	1.99	101.8
	21	40.0	43.5	17.5	0.18	0.41	81.6	2.00	101.8
	22	40.0	43.7	17.3	0.18	0.41	81.8	2.00	101.8
	24	39.7	43.9	17.0	0.18	0.41	82.2	1.99	101.4
	28	40.0	44.0	16.6	0.16	0.42	82.5	2.00	101.4

Table A1-3: Continued.

Sample	Analysis No.	SiO_2 (wt %)	MgO (wt %)	FeO (wt %)	MnO (wt %)	NiO (wt %)	Fo (#)	Cations (mol)	Total (wt %)
	29	39.8	44.1	16.4	0.17	0.44	82.8	1.99	101.2
	31	40.2	44.6	16.3	0.16	0.43	83.0	2.01	101.9
	32	40.1	44.4	16.2	0.16	0.43	83.0	2.00	101.6
	33	40.1	44.8	16.2	0.16	0.43	83.2	2.01	101.9
	34	40.2	44.7	16.2	0.16	0.44	83.1	2.01	102.0
	35	40.2	44.5	16.2	0.16	0.43	83.1	2.01	101.7
	36	40.1	44.6	16.3	0.17	0.43	83.0	2.01	101.9
	37	40.2	44.4	16.4	0.16	0.43	82.8	2.01	101.9
	38	40.1	44.4	16.5	0.17	0.43	82.8	2.01	101.9
	39	39.9	44.2	16.7	0.17	0.42	82.5	2.00	101.6
	41	40.0	43.8	17.2	0.18	0.41	82.0	2.00	101.9
	42	39.9	43.3	17.8	0.19	0.41	81.3	1.99	101.8
75-Nii-2-4	1	39.5	41.1	20.5	0.23	0.34	78.1	1.97	101.7
	2	39.4	41.4	20.1	0.22	0.35	78.6	1.97	101.7
	3	39.6	41.7	19.4	0.21	0.36	79.3	1.97	101.5
	4	39.5	42.1	18.8	0.20	0.38	79.9	1.97	101.2
	5	39.6	42.1	18.2	0.19	0.40	80.5	1.97	101.0
	7	39.8	43.2	17.4	0.17	0.41	81.5	1.98	101.3
	8	39.9	43.3	17.1	0.17	0.40	81.9	1.98	101.2
	11	40.2	44.1	16.5	0.15	0.42	82.7	2.00	101.6
	12	40.1	44.2	16.2	0.15	0.43	82.9	2.00	101.4
	13	40.1	44.2	16.1	0.15	0.43	83.0	2.00	101.3
	14	40.2	44.4	15.9	0.15	0.42	83.2	2.00	101.3
	15	40.1	44.5	15.8	0.15	0.42	83.4	2.00	101.2
	16	40.2	44.5	15.5	0.14	0.43	83.6	2.00	101.1

Table A1-3: Continued.

Sample	Analysis No.	SiO_2 (wt %)	MgO (wt %)	FeO (wt %)	MnO (wt %)	NiO (wt %)	Fo (#)	Cations (mol)	Total (wt %)
	17	40.2	44.6	15.6	0.14	0.44	83.6	2.00	101.2
	18	40.2	44.8	15.4	0.14	0.43	83.9	2.00	101.1
	19	40.3	44.8	15.2	0.14	0.44	84.0	2.00	101.1
	20	40.3	44.9	15.0	0.14	0.43	84.2	2.00	100.9
	21	40.2	44.7	14.9	0.14	0.44	84.2	1.99	100.9
	22	40.3	45.0	14.9	0.14	0.45	84.3	2.00	101.0
	23	40.2	45.1	14.8	0.14	0.44	84.4	2.00	100.9
	24	40.2	45.0	14.8	0.13	0.44	84.4	2.00	100.9
	25	40.3	44.9	14.9	0.14	0.45	84.3	2.00	100.9
	26	40.1	44.7	15.2	0.14	0.45	84.0	2.00	100.9
	27	40.1	44.4	15.7	0.15	0.44	83.5	2.00	101.1
	28	40.0	43.8	16.4	0.16	0.43	82.6	1.99	101.0
	30	39.5	42.3	18.3	0.19	0.41	80.5	1.97	100.9
	31	39.4	41.4	19.3	0.20	0.39	79.3	1.96	100.9
	32	39.1	40.5	20.6	0.23	0.35	77.8	1.95	100.9
75-Nii-2-5	1	39.2	39.5	23.0	0.27	0.26	75.4	2.00	102.3
	2	38.9	39.5	22.5	0.25	0.27	75.8	2.00	101.6
	4	39.0	40.1	21.3	0.24	0.31	77.1	2.00	101.3
	5	39.4	40.9	20.7	0.23	0.32	77.9	2.00	101.8
	6	39.7	41.8	20.0	0.21	0.35	78.8	1.99	102.2
	7	39.5	41.9	19.4	0.21	0.34	79.3	2.00	101.6
	8	39.6	42.3	19.0	0.20	0.36	79.9	2.00	101.6
	10	40.1	43.4	17.6	0.17	0.36	81.5	2.00	101.8
	11	40.1	43.5	16.9	0.17	0.37	82.1	2.00	101.8
	12	40.4	44.6	16.6	0.17	0.38	82.7	2.00	102.3

Table A1-3: Continued.

Sample	Analysis No.	SiO_2 (wt %)	MgO (wt %)	FeO (wt %)	MnO (wt %)	NiO (wt %)	Fo (#)	Cations (mol)	Total (wt %)
	13	40.3	44.6	16.2	0.16	0.38	83.1	2.01	101.9
	14	40.2	44.5	16.1	0.16	0.38	83.1	2.00	101.6
	15	40.2	44.5	16.2	0.17	0.39	83.0	2.01	101.7
	17	40.1	43.8	17.2	0.18	0.37	82.0	2.00	101.9
	18	40.0	43.1	18.1	0.19	0.37	80.9	1.99	102.0
	20	39.6	41.3	20.4	0.23	0.34	78.3	1.98	102.1
	21	39.3	40.1	21.5	0.25	0.31	76.9	1.96	101.7
	22	39.0	39.4	22.7	0.26	0.29	75.6	1.95	101.9
75-Nii-2-6	5	40.0	43.5	17.3	0.19	0.39	81.7	1.99	101.7
	9	40.5	45.9	14.5	0.13	0.40	85.0	2.02	101.7
	10	40.5	46.2	14.3	0.14	0.40	85.2	2.03	101.7
	11	40.6	46.3	14.1	0.13	0.40	85.4	2.03	101.8
	14	40.6	46.3	13.8	0.13	0.40	85.6	2.02	101.6
	15	40.6	46.4	13.9	0.13	0.40	85.6	2.03	101.7
	16	40.6	46.4	14.0	0.13	0.40	85.6	2.03	101.8
	19	40.4	46.2	14.2	0.13	0.40	85.3	2.02	101.5
	20	40.5	46.1	14.1	0.13	0.40	85.3	2.02	101.6
	22	40.6	46.2	14.2	0.13	0.40	85.3	2.03	101.8
	23	40.5	46.0	14.2	0.13	0.41	85.2	2.02	101.6
	24	40.4	46.1	14.3	0.13	0.41	85.2	2.02	101.6
	26	40.5	45.9	14.5	0.13	0.41	85.0	2.02	101.8
	30	40.3	46.1	14.5	0.13	0.41	85.0	2.02	101.7
	32	40.6	45.9	14.7	0.14	0.40	84.7	2.03	102.0
	34	40.4	45.7	15.1	0.14	0.39	84.4	2.02	102.0
	36	40.3	45.3	15.6	0.15	0.39	83.8	2.02	102.0

Table A1-3: Continued.

Sample	Analysis No.	SiO_2 (wt %)	MgO (wt %)	FeO (wt %)	MnO (wt %)	NiO (wt %)	Fo (#)	Cations (mol)	Total (wt %)
	37	40.2	45.0	16.0	0.16	0.37	83.4	2.02	101.9
	38	40.2	44.6	16.4	0.16	0.37	82.9	2.01	102.0
	39	40.1	44.2	16.8	0.16	0.37	82.4	2.01	101.9
	41	39.9	43.4	17.8	0.19	0.36	81.3	2.00	101.9
	42	39.6	43.1	18.1	0.20	0.36	80.9	1.99	101.7
	43	39.8	42.8	18.6	0.20	0.35	80.4	1.99	101.9
	44	39.6	42.5	18.8	0.21	0.35	80.1	1.98	101.7
75-Nii-2-7	1	39.0	40.4	21.2	0.24	0.30	77.2	1.95	101.5
	3	39.5	41.4	20.2	0.22	0.33	78.5	1.97	102.0
	4	39.6	41.7	19.9	0.21	0.33	78.9	1.98	101.9
	5	39.6	41.9	19.5	0.21	0.34	79.3	1.98	101.8
	6	39.7	42.0	19.4	0.21	0.33	79.4	1.98	101.9
	7	39.6	42.0	19.3	0.22	0.33	79.5	1.98	101.8
	8	39.6	41.7	19.5	0.21	0.33	79.3	1.97	101.7
	9	39.6	41.8	19.6	0.21	0.33	79.2	1.98	101.8
	10	39.5	41.5	20.0	0.22	0.32	78.7	1.97	101.7
	11	39.3	41.0	20.2	0.23	0.32	78.3	1.96	101.4
	12	39.3	41.0	20.4	0.23	0.31	78.2	1.96	101.5
	13	39.4	40.7	20.4	0.23	0.32	78.1	1.96	101.3
	14	39.4	40.8	20.8	0.24	0.31	77.8	1.97	101.8
	16	39.4	40.8	21.0	0.24	0.32	77.6	1.97	102.0
	18	39.3	40.4	21.5	0.25	0.29	77.0	1.96	102.0
	19	39.2	40.1	21.7	0.25	0.28	76.7	1.96	101.7
	21	38.9	39.2	22.5	0.26	0.27	75.6	1.94	101.4
	23	38.9	38.7	23.4	0.29	0.26	74.7	1.94	101.9

Table A1-3: Continued.

Sample	Analysis No.	SiO_2 (wt %)	MgO (wt %)	FeO (wt %)	MnO (wt %)	NiO (wt %)	Fo (#)	Cations (mol)	Total (wt %)
	24	38.9	38.6	23.5	0.29	0.26	74.6	1.94	101.7
	25	38.7	38.3	23.9	0.29	0.25	74.1	1.93	101.6
	26	38.7	37.9	24.2	0.29	0.24	73.6	1.93	101.6
75-Nii-2-8	1	40.1	42.9	18.1	0.21	0.38	80.8	1.99	101.9
	3	40.1	43.5	17.6	0.20	0.39	81.5	2.00	102.0
	4	40.1	43.7	17.3	0.19	0.39	81.8	2.00	101.9
	5	40.2	44.0	16.8	0.17	0.39	82.4	2.00	101.8
	6	40.4	44.5	16.3	0.17	0.40	82.9	2.01	102.0
	7	40.3	44.8	15.9	0.15	0.41	83.4	2.01	101.8
	8	40.4	45.0	15.5	0.15	0.40	83.8	2.01	101.8
	9	40.5	45.2	15.3	0.16	0.41	84.1	2.02	101.8
	10	40.6	45.5	14.9	0.14	0.42	84.5	2.02	101.8
	11	40.6	45.7	14.7	0.14	0.42	84.7	2.02	101.8
	12	40.4	45.7	14.6	0.15	0.43	84.8	2.02	101.6
	13	40.6	46.0	14.6	0.14	0.42	84.9	2.03	101.9
	14	40.4	46.0	14.4	0.15	0.42	85.0	2.02	101.6
	15	40.7	45.9	14.5	0.15	0.43	85.0	2.03	102.0
	16	40.8	45.9	14.5	0.14	0.44	84.9	2.03	102.5
	17	40.4	45.8	14.7	0.15	0.42	84.8	2.02	101.7
	18	40.6	45.6	14.9	0.15	0.42	84.5	2.02	101.9
	20	40.5	45.1	15.5	0.16	0.41	83.9	2.02	102.0
	21	40.3	44.8	16.1	0.17	0.41	83.3	2.01	102.0
	22	39.9	44.3	16.5	0.17	0.39	82.7	2.00	101.6
	25	40.0	43.1	18.0	0.21	0.36	81.0	1.99	102.0
	26	39.7	42.6	18.6	0.21	0.36	80.3	1.98	101.8

Table A1-3: Continued.

Sample	Analysis No.	SiO_2 (wt %)	MgO (wt %)	FeO (wt %)	MnO (wt %)	NiO (wt %)	Fo (#)	Cations (mol)	Total (wt %)
75-Nii-2-9	1	39.6	41.6	19.8	0.23	0.34	78.9	1.97	101.8
	2	39.7	42.1	19.2	0.21	0.36	79.7	1.98	101.8
	3	39.9	42.8	18.4	0.20	0.37	80.6	1.99	101.8
	4	39.7	43.2	17.5	0.19	0.39	81.5	1.98	101.3
	6	40.2	44.5	16.3	0.18	0.41	83.0	2.01	101.8
	7	40.3	44.8	15.8	0.16	0.42	83.5	2.01	101.7
	9	40.5	45.6	14.9	0.15	0.41	84.5	2.02	101.8
	11	40.5	46.0	14.1	0.15	0.42	85.3	2.02	101.5
	12	40.5	46.3	14.0	0.14	0.43	85.5	2.03	101.6
	14	40.6	46.3	13.8	0.14	0.42	85.6	2.02	101.5
	15	40.5	46.5	13.7	0.14	0.42	85.8	2.03	101.6
	16	40.6	46.7	13.4	0.14	0.43	86.1	2.03	101.5
	17	40.7	46.8	13.4	0.13	0.43	86.1	2.03	101.8
	18	40.7	46.8	13.4	0.13	0.43	86.2	2.03	101.8
	19	40.6	46.7	13.3	0.14	0.42	86.2	2.03	101.4
	20	40.5	46.7	13.3	0.13	0.42	86.2	2.03	101.4
	21	40.7	46.8	13.3	0.13	0.42	86.3	2.03	101.6
	22	40.7	47.0	13.3	0.13	0.42	86.3	2.04	101.7
	24	40.8	47.1	13.2	0.12	0.42	86.4	2.04	101.9
	28	40.8	47.0	13.3	0.14	0.42	86.3	2.04	101.9
	29	40.7	47.0	13.3	0.13	0.42	86.3	2.04	101.7
	30	40.7	46.7	13.2	0.14	0.43	86.3	2.03	101.6
	31	40.8	46.9	13.2	0.13	0.42	86.3	2.03	101.8
	32	40.7	46.7	13.3	0.13	0.42	86.3	2.03	101.7
	33	40.8	46.8	13.3	0.13	0.42	86.2	2.03	101.8
	34	40.7	46.7	13.3	0.13	0.42	86.2	2.03	101.5

Table A1-3: Continued.

Sample	Analysis No.	SiO_2 (wt %)	MgO (wt %)	FeO (wt %)	MnO (wt %)	NiO (wt %)	Fo (#)	Cations (mol)	Total (wt %)
	35	40.8	46.8	13.4	0.13	0.41	86.1	2.03	101.8
	37	40.6	46.6	13.5	0.12	0.42	86.0	2.03	101.5
	38	40.7	46.6	13.7	0.13	0.43	85.8	2.03	101.8
	39	40.0	46.5	14.0	0.14	0.42	85.5	2.02	101.3
Average									
75-Nii-2-1		39.3	43.8	15.2	0.16	0.39	83.6	1.96	99.1
75-Nii-2-2		39.2	42.7	16.6	0.18	0.38	82.0	1.95	99.3
75-Nii-2-3		39.8	43.2	17.8	0.19	0.40	81.2	1.99	101.6
75-Nii-2-4		39.9	43.6	16.7	0.16	0.41	82.3	1.99	101.1
75-Nii-2-5		39.7	42.1	19.2	0.21	0.34	79.6	1.99	101.8
75-Nii-2-6		40.3	45.3	15.4	0.15	0.39	83.9	2.02	101.8
75-Nii-2-7		39.3	40.6	21.0	0.24	0.30	77.4	1.96	101.7
75-Nii-2-8		40.3	44.8	15.9	0.16	0.41	83.4	2.01	101.9
75-Nii-2-9		40.5	45.9	14.4	0.15	0.41	85.0	2.02	101.7

A2: Bulk olivine Mg-Fe isotopic and major elemental data

Table A2-1: Bulk olivine sample details for Mauna Kea (HSDP), Kahoolawe, and Niihau.

Sample	Weight (mg)	Comments*
Mauna Kea (HSDP)		All grains have dark green to light green color unless noted.
HSDP-284-1	1.0	~4 small melt inclusions observable.
HSDP-284-2	1.5	~5 large melt inclusions along with >10 smaller inclusions observable.
HSDP-284-3	6.7	2 large melt inclusions observable. Grain diameter >>1 mm.
HSDP-284-4	1.8	>10 small melt inclusions observable.
HSDP-284-5	1.4	~2 small melt inclusions observable.
HSDP-284-6	2.8	~2 small melt inclusions observable.
HSDP-284-7	1.7	~3 large melt inclusions along with >10 smaller inclusions observable.
HSDP-284-8	6.3	~5 large melt inclusions. Grain diameter >>1mm.
HSDP-284-9	1.8	1 large melt inclusion with >10 smaller inclusions observable.
HSDP-284-10	12.8	>10 small melt inclusions observable. Grain diameter >>1mm.
HSDP-284-11	2.8	~2 small melt inclusions observable.
HSDP-284-12	2.7	>10 small melt inclusions observable.
HSDP-284-13	3.0	2 large melt inclusions with >10 smaller inclusions observable.
HSDP-284-14	1.0	No observable inclusions. Grain diameter <<1mm.
HSDP-284-15	1.3	No observable inclusions. Grain diameter <<1mm.
HSDP-284-16	0.9	~1 small melt inclusion observable.
HSDP-284-17	1.1	No observable inclusions.
HSDP-284-18	8.1	2 large melt inclusions with >10 smaller inclusions observable.
HSDP-284-19	6.2	~5 small melt inclusions observable.
HSDP-284-20	1.5	~5 small melt inclusions observable.

Sample	Weight (mg)	Comments
Niihau		All grains have yellow-gold color with patches of orange unless noted.
75-Nii-4-1	0.8	Granular texture and dark green color observable.
75-Nii-4-2	0.5	Small dark lineations present within grain.
75-Nii-4-3	0.3	Granular texture with >10 small melt inclusions observable. Grain size <<1mm.
75-Nii-4-4	0.3	Grain size <<1mm.
75-Nii-4-5	1.8	No observable inclusions.
75-Nii-4-6	0.9	1 large melt inclusion present.
75-Nii-4-9	1.1	Grain appears lightly altered.
75-Nii-4-10	0.6	Grain appears moderately altered (red coloration present). >10 small melt inclusions observable.
75-Nii-4-13	0.4	Grain appears lightly altered. Granular texture with >10 small melt inclusions observable.
75-Nii-4-14	0.6	Grain appears lightly altered. Large dark lineation observable.
75-Nii-4-15	0.6	Grain appears moderately altered (brown coloration present). Grain size <<1mm.
Kahoolawe		All grains have light-yellow to green color unless noted.
Kah-16-1	1.5	~8 large melt inclusions and one possible garnet inclusion observable.
Kah-16-2	1.3	~5 small melt inclusions and one dark lineation observable.
Kah-16-3	2.0	1 large melt inclusion observable.
Kah-16-4	1.5	>10 small melt inclusions observable.
Kah-16-5	6.0	3 large melt inclusions observable. Grain size >>1mm.
Kah-16-6	0.9	3 large melt inclusions observable, one being a possible garnet or spinel inclusion.
Kah-16-7	5.7	3 large melt inclusions and >10 smaller inclusions observable. Grain size >>1mm.
Kah-16-8	3.2	5 garnet-like inclusions and >20 small melt inclusions observable.
Kah-16-9	1.2	2 large melt inclusions with >20 smaller inclusions observable.
Kah-16-10	1.8	3 garnet-like inclusions and >20 small melt inclusions observable.
Kah-16-11	0.9	1 spinel-like inclusion and >10 small melt inclusions observable.
Kah-16-12	0.9	1 large melt inclusion with ~3-4 smaller inclusions observable.
Kah-16-13	1.2	Granular texture and 1 large melt inclusion observable.

Table A2-1: Continued.

Sample	Weight (mg)	Comments
Kah-16-14	0.8	~7 large melt inclusions (several having garnetoid features) with ~3 smaller inclusions observable.
Kah-16-15	1.5	2 large melt inclusions with >10 smaller inclusions observable.
Kah-16-16	1.7	1 large melt inclusion with >10 smaller inclusions observable.
Kah-16-17	0.8	Granular texture and ~5 small melt inclusions observable.
Kah-16-18	1.0	1 large melt inclusion and ~2-3 smaller inclusions observable.
Kah-16-19	2.4	Granular texture and 3 large melt inclusions with >20 smaller inclusions observable.
Kah-16-20	6.6	Possible alteration. 3 large melt inclusions observable. Grain size >>1mm.
Kah-16-21	1.1	~5 large melt inclusions with >10 smaller inclusions observable.
Kah-16-22	5.6	~5 large melt inclusions with >30 smaller inclusions observable. Grain size >>1mm.

*Large melt inclusions >50 μm in diameter and small melt inclusions <50 μm in diameter.

Table A2-2: Bulk olivine Mg-Fe isotopic and major elemental data for standards, Mauna Kea (HSDP), Kahoolawe, and Niihau.

Sample*	n (repeat analyses)	δ^{56}Fe (‰)	2 SD	δ^{57}Fe (‰)	2 SD	δ^{25}Mg (‰)	2 SD	δ^{26}Mg (‰)	2 SD	Fo (#)
Standards						**		**		
BHVO-2	3	0.084	0.004	0.151	0.083	-0.117	0.016	-0.209	0.035	56
DTS-2	3	0.007	0.023	0.035	0.099	-0.138	0.034	-0.264	0.017	94
PCC-1	3	0.003	0.004	0.009	0.063	-0.126	0.013	-0.240	0.044	92
BCR-2	3	0.085	0.031	0.110	0.120	-0.065	0.047	-0.118	0.052	41
BIR-1	3	0.048	0.040	0.102	0.056	-0.105	0.026	-0.221	0.031	64
Mauna Kea (HSDP)										
HSDP-284-1	3	-0.234	0.037	-0.379	0.027	-0.140	0.015	-0.289	0.012	90
HSDP-284-2	3	0.071	0.049	0.130	0.076	-0.156	0.004	-0.319	0.019	87
HSDP-284-3	3	-0.065	0.037	-0.093	0.134	-0.119	0.013	-0.248	0.009	90
HSDP-284-4	3	-0.086	0.009	-0.116	0.084	-0.144	0.022	-0.279	0.028	91
HSDP-284-5	3	-0.056	0.046	-0.065	0.079	-0.151	0.019	-0.273	0.017	89
HSDP-284-6	3	-0.104	0.033	-0.128	0.056	-0.143	0.022	-0.276	0.011	90
HSDP-284-7	3	0.065	0.051	0.083	0.057	-0.151	0.026	-0.274	0.010	87
HSDP-284-8	3	-0.092	0.035	-0.144	0.084	-0.131	0.009	-0.252	0.012	91
HSDP-284-9	3	-0.041	0.054	-0.084	0.128	-0.157	0.045	-0.267	0.033	90
HSDP-284-10	3	-0.010	0.023	0.006	0.050	-0.132	0.009	-0.243	0.009	89
HSDP-284-10R	3	-0.008	0.015	0.002	0.077	-0.141	0.016	-0.278	0.031	-
HSDP-284-11	3	-0.096	0.053	-0.165	0.116	-0.119	0.003	-0.250	0.023	90
HSDP-284-12	3	-0.169	0.009	-0.259	0.109	-0.152	0.024	-0.278	0.024	89
HSDP-284-13	3	0.035	0.038	0.030	0.033	-0.145	0.022	-0.295	0.027	89
HSDP-284-14	3	-0.117	0.035	-0.186	0.138	-0.146	0.024	-0.277	0.028	90
HSDP-284-15	3	0.022	0.032	0.004	0.097	-0.155	0.023	-0.290	0.022	89
HSDP-284-16	3	-0.080	0.016	-0.109	0.025	-0.138	0.008	-0.278	0.044	90
HSDP-284-17	3	-0.078	0.019	-0.141	0.095	-0.127	0.026	-0.255	0.023	91

Table A2-2: Continued.

Sample	n (repeat analyses)	δ^{56}Fe (‰)	2 SD	δ^{57}Fe (‰)	2 SD	δ^{25}Mg (‰)	2 SD	δ^{26}Mg (‰)	2 SD	Fo (#)
HSDP-284-18	3	-0.053	0.024	-0.122	0.042	-0.141	0.005	-0.281	0.049	90
HSDP-284-19	3	0.008	0.024	-0.005	0.083	-0.155	0.020	-0.279	0.026	90
HSDP-284-19R	3	-0.004	0.068	-0.038	0.149	-0.141	0.012	-0.279	0.024	-
HSDP-284-20	3	-0.123	0.017	-0.169	0.108	-0.155	0.023	-0.285	0.021	90
Niihau										
75-Nii-4-1	3	-1.706	0.044	-2.531	0.105	0.171	0.032	0.356	0.022	81
75-Nii-4-2	3	-1.201	0.044	-1.765	0.072	0.130	0.033	0.248	0.022	78
75-Nii-4-3	3	-0.328	0.036	-0.507	0.119	0.001	0.016	0.019	0.018	71
75-Nii-4-4	3	-0.815	0.060	-1.217	0.064	0.050	0.041	0.108	0.017	78
75-Nii-4-5	3	-0.957	0.023	-1.406	0.078	-0.029	0.030	-0.012	0.032	85
75-Nii-4-5R	3	-0.971	0.047	-1.459	0.072	-0.021	0.040	-0.023	0.009	-
75-Nii-4-6	3	-0.363	0.023	-0.543	0.142	-0.022	0.031	-0.060	0.042	80
75-Nii-4-9	3	-0.979	0.050	-1.486	0.074	0.081	0.009	0.123	0.045	80
75-Nii-4-10	3	-0.557	0.037	-0.855	0.087	-0.059	0.024	-0.130	0.025	84
75-Nii-4-13	3	-0.726	0.034	-1.122	0.072	0.027	0.039	0.063	0.021	78
75-Nii-4-14	3	-0.760	0.032	-1.102	0.049	-0.030	0.011	-0.058	0.046	83
75-Nii-4-15	3	-1.115	0.062	-1.656	0.112	0.079	0.006	0.196	0.023	80
Kahoolawe										
Kah-16-1	3	-0.125	0.031	-0.217	0.071	-0.139	0.026	-0.273	0.040	88
Kah-16-2	3	-0.294	0.010	-0.411	0.095	-0.123	0.062	-0.248	0.053	86
Kah-16-3	3	0.021	0.045	0.004	0.071	-0.144	0.028	-0.283	0.032	89
Kah-16-4	3	-0.138	0.047	-0.217	0.136	-0.133	0.020	-0.248	0.014	88
Kah-16-5	3	-0.017	0.033	-0.034	0.027	-0.138	0.029	-0.280	0.029	88
Kah-16-6	3	-0.086	0.019	-0.138	0.083	-0.124	0.018	-0.255	0.008	88
Kah-16-7	3	-0.064	0.039	-0.101	0.063	-0.137	0.015	-0.270	0.037	88
Kah-16-7R	3	-0.064	0.037	-0.123	0.115	-0.124	0.016	-0.269	0.043	-

Table A2-2: Continued.

Sample	n (repeat analyses)	δ^{56}Fe (‰)	2 SD	δ^{57}Fe (‰)	2 SD	δ^{25}Mg (‰)	2 SD	δ^{26}Mg (‰)	2 SD	Fo (#)
Kah-16-8	3	-0.216	0.016	-0.374	0.087	-0.113	0.008	-0.231	0.050	89
Kah-16-9	3	-0.153	0.033	-0.249	0.077	-0.115	0.043	-0.239	0.030	87
Kah-16-10	3	-0.055	0.021	-0.072	0.049	-0.136	0.032	-0.285	0.001	88
Kah-16-11	3	-0.101	0.037	-0.132	0.137	-0.151	0.012	-0.293	0.034	86
Kah-16-12	3	-0.197	0.023	-0.262	0.061	-0.140	0.022	-0.263	0.019	86
Kah-16-13	3	-0.452	0.025	-0.660	0.058	-0.082	0.051	-0.176	0.017	87
Kah-16-14	9	-0.402	0.075	-0.562	0.033	-0.088	0.010	-0.169	0.015	87
Kah-16-15	3	-0.275	0.031	-0.369	0.123	-0.118	0.012	-0.249	0.020	85
Kah-16-16	3	-0.254	0.035	-0.398	0.142	-0.123	0.040	-0.222	0.011	87
Kah-16-17	3	-0.206	0.042	-0.304	0.060	-0.116	0.034	-0.237	0.036	87
Kah-16-18	3	-0.517	0.050	-0.781	0.064	-0.066	0.020	-0.122	0.015	87
Kah-16-19	3	-0.001	0.031	0.011	0.101	-0.127	0.073	-0.249	0.045	84
Kah-16-20	3	-0.166	0.028	-0.250	0.097	-0.127	0.020	-0.245	0.044	88
Kah-16-20R	3	-0.205	0.040	-0.225	0.050	-0.122	0.012	-0.241	0.039	-
Kah-16-21	3	-0.204	0.043	-0.295	0.054	-0.123	0.025	-0.253	0.009	88
Kah-16-22	3	-0.078	0.025	-0.074	0.047	-0.132	0.002	-0.245	0.040	88

*R denotes replicate of a given sample from isotopic analysis.

**Mg sample solution processed twice through column.

A3: Summary of literature data

- **Figure 6** contains basalt whole-rock data from Cousens and Clague (2015). The samples were collected from a variety of basaltic formations from Kauai and Niihau islands, which include shield and post-shield lavas for Kauai and shield, late-shield, and post-shield lavas for Niihau (the Ni anomaly being reported in a late-shield lava).

- Other than the locations described in Sobolev et al. (2007), **Figure 7** contains olivine data from the following locations, where [1] = Putirka et al. (2011), [2] = Oeser et al. (2015), and [3] = Hartley et al. (2016):

WPM-Thick:

HSDP-2, Mauna Kea volcano, Hawaii. [1]

Massif Central, France. [2]

MORB:

Siqueiros transform fault, Pacific Ocean. [1]

WPM-Thin:

Laki fissure, Eastern Volcanic Zone, Iceland. [3]

- **Figures 8**, **9**, and **10** contain olivine data from Teng et al. (2011) (three Hawaiian locations: Koolau range, Loihi seamount, and Kilauea Iki lava lake) and Sio et al. (2013) [Kilauea Iki lava lake, as in Teng et al. (2011)].

Appendix B: Fractional crystallization model

The olivine fractional crystallization model is based partially on that of Putirka et al. (2011) (see their Appendix B: olivine crystal lines of descent). This model allows for the composition of a given olivine crystallizing out of a melt to be estimated using solely the initial composition of the melt. This is done by progressively subtracting out the composition of the olivine from that of the melt each time it crystallizes in equilibrium with the melt. An initial normalized (to 100 wt %) composition of a typical ocean-island basalt is used here as the initial melt composition (**Table B1**; being used for the fractional crystallization models of **Figure 7**). The molar Fe/Mg ratio is first calculated for the melt and then converted to that of an olivine which would crystallize in equilibrium with the melt. This is done by assuming that the olivine/melt partition coefficient of Fe/Mg is a constant equal to 0.32 [similar to the value used in Rhodes et al. (2012)]:

$$K_D\,(\text{Fe-Mg})^{\text{ol-melt}} = 0.32$$

Therefore, the olivine molar Fe/Mg ratio can be calculated:

$$\text{Fe/Mg}_{\,(\text{ol})} = K_D\,(\text{Fe-Mg})^{\text{ol-melt}}\,(\text{Fe/Mg})_{\,(\text{melt})} = 0.32\,(\text{Fe/Mg})_{\,(\text{melt})}$$

By knowing the molar Fe/Mg ratio of the olivine, the molar proportions of the oxides in olivine [$(Mg,Fe)_2SiO_4$] can be determined (as shown in **Table B2**). Following this, conversion to wt % composition is simple:

$XO\ (\text{wt \%}) = A_xM_{x,}$ where A = atomic mass and M = molar proportion of oxide XO

Following renormalization, olivine Ni content will need to be calculated. This requires that its olivine/melt partition coefficient be determined, which can be estimated by the Mg

Table B1: Typical ocean-island basalt composition.

	FeO_T* (wt %)	MgO (wt %)	SiO_2 (wt %)	TiO_2 (wt %)	Al_2O_3 (wt %)	MnO (wt %)	CaO (wt %)	Na_2O (wt %)	NiO (wt %)	Total (wt %)	Fe/Mg (mole)
Initial melt	10.58	19.27	48.05	1.94	9.88	0.17	8.16	1.68	0.15	100.00	0.27

*FeO as total Fe (i.e. FeO + Fe_2O_3).

Table B2: Calculation of olivine composition from composition of **Table B1**.

Olivine/melt	D (Mg)	D (Ni)
	2.62	5.09

Olivine		Fe/Mg (mole)	Fe (mole)	Mg (mole)	SiO_2 (mole)	Fo (#)
	Molar proportion	0.09	0.16	1.84	1.00	91.92
		FeO (wt %)	MgO (wt %)	SiO_2 (wt %)	NiO* (wt %)	Total (wt %)
	Composition	11.70	74.04	60.08	0.77	146.60
	Renormalized	7.96	50.39	40.89	0.76	100.00

*Added in and renormalized following determination of other compositions.

olivine/melt partition coefficient using Eq. 13 of Beattie (1993) (parameters from his Table 1):

$$K_D\,(Ni)^{ol\text{-}melt} = 3.346\,K_D\,(Mg)^{ol\text{-}melt} - 3.665$$

By knowing the Ni partition coefficient, olivine NiO composition can be readily determined:

$$NiO_{ol}\ (wt\ \%) = K_D\,(Ni)^{ol\text{-}melt}\ NiO_{melt}\ (wt\ \%)$$

Afterwards, each composition is renormalized to 100 wt % with respect to NiO (**Table B2**).

Once the equilibrium olivine composition has been determined, the initial basalt composition is subtracted by 0.5% of each olivine compositional value (FeO, MgO, SiO_2, and NiO), followed by further renormalization to 100 wt %. This will result in a slight decrease in the olivine Fo composition as the olivine crystallized from the melt will become increasingly fayaltic (Fe-rich), as more Mg is removed by the olivine crystallization process. The olivine subtraction process is then progressively repeated in 0.5% increments until the desired equilibrium olivine composition is reached (in the case of the fractional crystallization models of **Figure 7**, this is approximately Fo_{80}). Note here that the complex parameters of oxygen fugacity, temperature, and pressure are assumed to be constant over the course of crystallization.

Appendix C: Chemical diffusion model

The chemical diffusion model is based on Eq. 6.18 of Crank (1975) and Eq. 8.6.7 of Albaréde (1996), which is defined as non-steady state diffusion of a sphere at a given concentration within a medium of fixed concentration. This approximates diffusion of a spherical homogenous olivine crystal within a magma body which is assumed to have a constant concentration over time with respect to the olivine. The equation itself is a solution of a partial differential equation termed the 'diffusion equation for radial flux with a constant diffusion coefficient':

$$\frac{\partial C}{\partial t} = D\left(\frac{\partial^2 C}{\partial r^2} + \frac{2}{r}\frac{\partial C}{\partial r}\right)$$

Equation 1: Diffusion equation for radial flux with a constant diffusion coefficient [Eq. 6.1 of Crank (1975)].

Upon substituting and solving **Eq. 1** with respect to a uniform sphere concentration over a fixed surface concentration (which can also be obtained by appropriate substitution into Eq. 4.16 of Crank, 1975), the general solution is:

$$\frac{C(r,t) - C_0}{C_s - C_0} = 1 + \frac{2a}{\pi r}\sum_{n=1}^{\infty}\frac{(-1)^n}{n}\sin\frac{n\pi r}{a}\exp\left(-n^2\pi^2\frac{Dt}{a^2}\right)$$

which can also be rearranged as:

$$C(r,t) = C_0 + (C_s - C_0)\left(1 + \frac{2a}{\pi r}\sum_{n=1}^{\infty}\frac{(-1)^n}{n}\sin\frac{n\pi r}{a}\exp\left(-n^2\pi^2\frac{Dt}{a^2}\right)\right)$$

Equation 2: Radial diffusion of a uniform sphere over a fixed surface concentration [modified from Eq. 6.18 of Crank (1975) and Eq. 8.6.10 of Albaréde (1996)].

This solution determines a concentration at a given time and location across the radius of a sphere; $C(r,t)$, where r is a point along the radius of the sphere and t is a point in time during diffusion of the sphere. C_0 is the initial concentration across the sphere, C_s is the fixed surface concentration of the medium, a is the radius of the sphere, and D is the diffusion coefficient, which is determined by the material being diffused (in this case, the mobile elements within olivine). The bulk concentration of the sphere can be determined by solving **Eq. 1** and integrating the solution with respect to volume to obtain:

$$C(t) = \frac{6C_0}{\pi^2}\sum_{n=1}^{\infty}\frac{1}{n^2}\exp\left(-n^2\pi^2\frac{Dt}{a^2}\right)$$

where $C_0 - C_s$ replaces C_0 and C_0 is added, similar to Eq. 5 of Lai et al. (2015):

$$C(t) = C_0 + \frac{6(C_0 - C_s)}{\pi^2}\sum_{n=1}^{\infty}\frac{1}{n^2}\exp\left(-n^2\pi^2\frac{Dt}{a^2}\right)$$

Equation 3: Bulk diffusion of a uniform sphere over a fixed surface concentration [modified from Eq. 8.6.7 of Albaréde (1996)].

where Dt/a^2 is varied instead of r as in **Eq. 2**.

Assuming that C_0 and C_s can be approximated by both the concentration of the core of the olivine and the concentration of the melt adjacent to the olivine rim, respectively, $C(r,t)$ can be calculated using **Eq. 2** by varying time at each location along the crystal radius. An example of the model can be seen in **Table C1**, which shows concentration of an element with D = $1.10e^{-17}$ across the radius of an olivine allowed to diffuse within a melt over a five year period. The olivine, with a C_0 of 15 (assumed here to be the measured elemental wt % within the olivine core), is placed into a melt of a C_s of 20 (assumed to be the measured elemental wt % of the melt near the olivine rim). While the concentration of the melt is higher than that of the olivine, it is only slightly enriched towards the core (i.e. for $0 < r < 0.00030$), whereas the concentration towards the rims experiences greater enrichment (i.e. for $0.00035 < r < 0.00040$). **Table C2** shows the same theoretical olivine-melt parameters across crystal radius with respect to a diffusing element, albeit with a diffusion time period increased to fifty years. By comparison, the concentration of the element across the olivine radius has greatly increased, with the inner core concentration (i.e. $r = 0$) increasing to ~16.7 (compared to the original 15). As a result, the element can be assumed to have diffused into the olivine from the melt with time, gradually increasing the concentration of the olivine to that of the melt. **Eq. 3** can be applied similarly, although Dt/a^2 is varied in place of r, with t determined by estimating D and a.

Using the olivine core composition, olivine rim composition, olivine radius length, and estimating diffusion coefficients within the range adopted from Chakraborty (1997) and Petry et al. (2004), **Eq. 2** was applied to the in-situ Mg, Fe, Ni, and Fo profiles of olivine 75-Nii-2-8 (**Figures 5** and **7**). Each initial parameter used is summarized in **Table C3**. t was varied along 1 month, 1 year, 10000 days (~27 years), and 50 years to illustrate the progression of diffusion of the elements within the olivine.

Table C1: Diffusion of an element in olivine over a five year period.

C_0 (wt %)	C_s (wt %)	a (meters)	D ($meters^2$/second)	t (seconds)
15	20	0.00040	$1.10e^{-17}$	$1.58e^{8}$

C (wt %)	15	15	15	15.00029	15.00685	15.08702	15.59704	17.26258	20
r (meters)	0	0.00005	0.00010	0.00015	0.00020	0.00025	0.00030	0.00035	0.00040

Table C2: Diffusion of the same element in olivine as in **Table C1** over a fifty year period.

C_0 (wt %)	C_s (wt %)	a (meters)	D ($meters^2$/second)	t (seconds)
15	20	0.00040	$1.10e^{-17}$	$1.58e^{9}$

C (wt %)	16.70783	16.78165	16.99990	17.35182	17.81659	18.36125	18.94123	19.50464	20
r (meters)	0	0.00005	0.00010	0.00015	0.00020	0.00025	0.00030	0.00035	0.00040

The diffusion model for the isotopic concentration of Mg and Fe (that is, δ^{26}Mg and δ^{56}Fe) takes into account the natural abundance of ^{26}Mg and ^{56}Fe relative to ^{24}Mg and ^{54}Fe, as natural abundance percentages are multiplied by C_0 and C_s for isotopic concentration. While D for the more common isotope is estimated (based on the range of published values), D for the less common isotope is calculated using Eq. 1 of Richter et al. (1999):

$$\frac{D_i}{D_j} = \left(\frac{m_j}{m_i}\right)^{\beta}$$

which can be reorganized to find D for the isotope of interest:

$$D_i = D_j \left(\frac{m_j}{m_i}\right)^{\beta}$$

Equation 4: Diffusion coefficient of an isotope i of an element [modified from Eq. 1 of Richter et al. (1999)].

where D_i and D_j refer to the diffusion coefficients of an element with isotopes of atomic mass m_i and m_j, respectively. β is an experimentally determined factor for olivine. Once isotopic profiles were determined for Mg and Fe, they were converted to δ^{26}Mg and δ^{56}Fe. For **Figure 5**, the estimated δ^{26}Mg-δ^{56}Fe profile of the olivine was created using **Eq. 2** and **4**, with varying timescale as in the major elemental diffusion models. **Eq. 3** and **4** were used to model δ^{26}Mg vs. δ^{56}Fe data (**Figure 10**). The data of **Figure 10** was also modeled using **Eq. 2** in order to show comparison between the radial and bulk diffusion models. Parameters for radial diffusion models used for **Figures 5**, **7**, and **10** are summarized in **Table C3**. Parameters for the bulk diffusion model used for **Figure 10** are summarized in **Table C4.**

Table C3: Parameters used for radial diffusion models of **Figures 5**, **7**, and **10**.

Element	C_0* (wt %, ppm for Ni)	C_s* (wt %, ppm for Ni)	a (meters)	D ($meters^2$/second)	β**
Mg	46.250	42.348	$4.040e^{-4}$	$1.100e^{-17}$ (for ^{24}Mg)	0.16
Fe	14.442	19.150	$4.040e^{-4}$	$1.100e^{-17}$ (for ^{56}Fe)	0.27
Ni	3378.260	2710.460	$4.040e^{-4}$	$1.100e^{-17}$	-

*Massif Central olivines adjusted to the high and low Fo compositions in **Figure 7**.

**Values from Sio et al. (2013).

Table C4: Parameters used for bulk diffusion model of **Figure 10**.

Element	C_0 (wt %, ppm for Ni)	C_s (wt %, ppm for Ni)	a (meters)	D ($meters^2$/second)	β*
Mg	46.250	37.500	$4.040e^{-4}$	$1.100e^{-17}$ (for ^{24}Mg)	0.16
Fe	16.000	27.500	$4.040e^{-4}$	$1.100e^{-17}$ (for ^{56}Fe)	0.27

*Values from Sio et al. (2013).

References cited

Albaréde, F., 1996, Introduction to Geochemical Modeling: Cambridge University Press, p. 419–460.

An, Y., Huang, J., Griffin, W.L., Liu, C., and Huang, F., 2017, Isotopic composition of Mg and Fe in garnet peridotites from the Kaapvaal and Siberian cratons: Geochimica et Cosmochimica Acta, v. 200, p. 167–185, doi: 10.1016/j.gca.2016.11.041.

An, Y., Wu, F., Xiang, Y., Nan, X., Yu, X., Yang, J., Yu, H., Xie, L., and Huang, F., 2014, High-precision Mg isotope analyses of low-Mg rocks by MC-ICP-MS: Chemical Geology, v. 390, p. 9–21, doi: 10.1016/j.chemgeo.2014.09.014.

Beattie, P., 1993, Olivine-melt and orthopyroxene-melt equilibria: Contributions to Mineralogy and Petrology, v. 115, p. 103–111, doi: 10.1007/BF00712982.

Beattie, P., Ford, C., and Russell, D., 1991, Partition coefficients for olivine-melt and orthopyroxene-melt systems: Contributions to Mineralogy and Petrology , v. 109, p. 212–224, doi: 10.1007/BF00306480.

Brandon, A.D., Walker, R.J., Puchtel, I.S., Becker, H., Humayun, M., and Revillon, S., 2003, ^{186}Os -^{187}Os systematics of Gorgona Island komatiites: implications for early growth of the inner core: Earth and Planetary Science Letters, v. 206, p. 411–426, doi: 10.1016/S0012-821X(02)01101-9.

Chakraborty, S., 1997, Rates and mechanisms of Fe-Mg interdiffusion in olivine at 980°-1300°C: Journal of Geophysical Research, v. 102, p. 12317–12331, doi: 10.1029/97jb00208.

Cousens, B.L., and Clague, D.A., 2015, Shield to Rejuvenated Stage Volcanism on Kauai and Niihau, Hawaiian Islands: Journal of Petrology, v. 56, p. 1547–1584, doi: 10.1093/petrology/egv045.

Crank, J., ed., 1975, Diffusion in a sphere, *in* The Mathematics of Diffusion, Second Edition: London, Oxford University Press, p. 89–103.

Dauphas, N., Teng, F.-Z., and Arndt, N.T., 2010, Magnesium and iron isotopes in 2.7 Ga Alexo komatiites: Mantle signatures, no evidence for Soret diffusion, and identification of diffusive transport in zoned olivine: Geochimica et Cosmochimica Acta, v. 74, p. 3274–3291, doi: 10.1016/j.gca.2010.02.031.

Dauphas, N., Craddock, P.R., Asimow, P.D., Bennett, V.C., Nutman, A.P., and Ohnenstetter, D., 2009, Iron isotopes may reveal the redox conditions of mantle melting from Archean to Present: Earth and Planetary Science Letters, v. 288, p. 255–267, doi: 10.1016/j.epsl.2009.09.029.

Dohmen, R., and Chakraborty, S., 2007, Fe-Mg diffusion in olivine II: Point defect chemistry, change of diffusion mechanisms and a model for calculation of diffusion coefficients in natural olivine: Physics and Chemistry of Minerals, v. 34, p. 409–430, doi: 10.1007/s00269-007-0158-6.

Gong, Y., Xia, Y., Huang, F., and Yu, H., 2016, Average iron isotopic compositions of the upper continental crust: constrained by loess from the Chinese Loess Plateau: Acta Geochimica, v. 36, p. 1–7, doi: 10.1007/s11631-016-0131-5.

Hartley, M.E., Morgan, D.J., Maclennan, J., Edmonds, M., and Thordarson, T., 2016, Tracking timescales of short-term precursors to large basaltic fissure eruptions through Fe–Mg diffusion in olivine: Earth and Planetary Science Letters, v. 439, p. 58–70, doi: 10.1016/j.epsl.2016.01.018.

Herzberg, C., Asimow, P.D., Ionov, D.A., Vidito, C., Jackson, M.G., and Geist, D., 2013, Nickel and helium evidence for melt above the core-mantle boundary: Nature, v. 493, p. 393–397, doi: 10.1038/nature11771.

Lai, Y.-J., Pogge von Strandmann, P.A.E., Dohmen, R., Takazawa, E., and Elliott, T., 2015, The influence of melt infiltration on the Li and Mg isotopic composition of the Horoman Peridotite Massif: Geochimica et Cosmochimica Acta, v. 164, p. 318–332, doi: 10.1016/j.gca.2015.05.006.

Oeser, M., Dohmen, R., Horn, I., Schuth, S., and Weyer, S., 2015, Processes and time scales of magmatic evolution as revealed by Fe–Mg chemical and isotopic zoning in natural olivines: Geochimica et Cosmochimica Acta, v. 154, p. 130–150, doi: 10.1016/j.gca.2015.01.025.

Pearce, T.H., 1987, The theory of zoning patterns in magmatic minerals using olivine as an example: Contributions to Mineralogy and Petrology, v. 97, p. 451–459, doi:10.1007/BF00375323.

Petry, C., Chakraborty, S., and Palme, H., 2004, Experimental determination of Ni diffusion coefficients in olivine and their dependence on temperature, composition, oxygen fugacity, and crystallographic orientation: Geochimica et Cosmochimica Acta, v. 68, p. 4179–4188, doi: 10.1016/j.gca.2004.02.024.

Putirka, K., Ryerson, F.J., Perfit, M., and Ridley, W.I., 2011, Mineralogy and Composition of the Oceanic Mantle: Journal of Petrology, v. 52, p. 279–313, doi: 10.1093/petrology/egq080.

Rhodes, J.M., Huang, S., Frey, F.A., Pringle, M., and Xu, G., 2012, Compositional diversity of Mauna Kea shield lavas recovered by the Hawaii Scientific Drilling Project: Inferences on source lithology, magma supply, and the role of multiple volcanoes: Geochemistry, Geophysics, Geosystems, v. 13, Q03014, p. 1-28, doi: 10.1029/2011GC003812.

Richter, F.M., Liang, Y., and Davis, A.M., 1999, Isotope fractionation by diffusion in molten oxides: Geochimica et Cosmochimica Acta, v. 63, p. 2853–2861, doi: 10.1016/S0016-7037(99)00164-7.

Shea, T., Lynn, K.J., and Garcia, M.O., 2015, Cracking the olivine zoning code: Distinguishing between crystal growth and diffusion: Geology, v. 43, p. 935–938, doi: 10.1130/G37082.1.

Sio, C.K.I., Dauphas, N., Teng, F.-Z., Chaussidon, M., Helz, R.T., and Roskosz, M., 2013, Discerning crystal growth from diffusion profiles in zoned olivine by in situ Mg–Fe isotopic analyses: Geochimica et Cosmochimica Acta, v. 123, p. 302–321, doi: 10.1016/j.gca.2013.06.008.

Sobolev, A.V., Hofmann, A.W., Kuzmin, D.V., Yaxley, G.M., Arndt, N.T., Chung, S.-L., Danyushevsky, L.V., Elliott, T., Frey, F.A., Garcia, M.O., Gurenko, A.A., Kamenetsky, V.S., Kerr, A.C., Krivolutskaya, N.A., Matvienkov, V.V., Nikogosian, I.K., Rocholl, A., Sigurdsson, I.A., Sushchevskaya, N.M., and Teklay, M., 2007, The amount of recycled crust in sources of mantle-derived melts: Science, v. 316, p. 412–417, doi: 10.1126/science.1138113.

Sobolev, A.V., Hofmann, A.W., Sobolev, S.V., and Nikogosian, I.K., 2005, An olivine-free mantle source of Hawaiian shield basalts: Nature, v. 434, p. 590–597, doi: 10.1038/nature03411.

Starr, F., and Starr, K., compilers, 2007, Stock Maps: State of Hawaii, 1 JPEG, http://www.hear.org/starr/maps/stock/originals/state_landsat_white.jpg, (accessed April 2017).

Teng, F.-Z., Dauphas, N., Huang, S., and Marty, B., 2013, Iron isotopic systematics of oceanic basalts: Geochimica et Cosmochimica Acta, v. 107, p. 12–26, doi: 10.1016/j.gca.2012.12.027.

Teng, F.-Z., Dauphas, N., Helz, R.T., Gao, S., and Huang, S., 2011, Diffusion-driven magnesium and iron isotope fractionation in Hawaiian olivine: Earth and Planetary Science Letters, v. 308, p. 317–324, doi: 10.1016/j.epsl.2011.06.003.

Teng, F., Li, W., Ke, S., Marty, B., Dauphas, N., Huang, S., Wu, F., and Pourmand, A., 2010, Magnesium isotopic composition of the Earth and chondrites: Geochimica et Cosmochimica Acta, v. 74, p. 4150–4166, doi: 10.1016/j.gca.2010.04.019.

Welsch, B., Hammer, J., and Hellebrand, E., 2014, Phosphorus zoning reveals dendritic architecture of olivine: Geology, v. 42, p. 867–870, doi: 10.1130/G35691.1.

Curriculum Vitae

Alexander James Valentine
Email: valena6@unlv.nevada.edu

Past Education:

- *University of California, Riverside*; B.S. in Geology, Cum Laude.

Awards & Honors:

- 04/2014: Los Angeles Basin Geological Society Scholarship.

- 04/2014: ConocoPhillips Scholarship.

- 05/2014: George Lapins UCR Earth Sciences Scholarship.

- 01/2016 & 02/2017: Edwards & Olswang UNLV Geoscience Scholarship.

- 06/2016: NSF East Asia and Pacific Summer Institutes for U.S. Graduate Students Grant (Award #1614148).

- 01/2017: UNLV Graduate Access Emergency Retention Grant.

- 01/2017: Bernada French UNLV Geoscience Scholarship.

Thesis Title:

An elemental highway: Investigation of a high nickel anomaly in olivine from the island of Niihau, Hawai‘i.